AMERICAN SOCIETY FOR MICROBIOLOGY | Molecular and Cellular Biology®

RESEARCH ARTICLE

Cxcl10 Chemokine Induces Migration of ING4-Deficient Breast Cancer Cells via a Novel Cross Talk Mechanism between the Cxcr3 and Egfr Receptors

Emily Tsutsumi,[a] Jeremiah Stricklin,[b] Emily A. Peterson,[b] Joyce A. Schroeder,[c] Suwon Kim[a,b,d]

[a]Clinical Translational Sciences Program, College of Medicine—Phoenix, University of Arizona, Phoenix, Arizona, USA
[b]Cancer and Cell Biology Division, Translational Genomics Research Institute, Phoenix, Arizona, USA
[c]Molecular and Cellular Biology, University of Arizona, Tucson, Arizona, USA
[d]Basic Medical Sciences, College of Medicine—Phoenix, University of Arizona, Phoenix, Arizona, USA

ABSTRACT The chemokine Cxcl10 has been associated with poor prognosis in breast cancer, but the mechanism is not well understood. Our previous study has shown that *CXCL10* was repressed by the ING4 tumor suppressor, suggesting a potential inverse functional relationship. We thus investigated a role for Cxcl10 in the context of ING4 deficiencies in breast cancer. We first analyzed public gene expression data sets and found that patients with *CXCL10*-high/*ING4*-low expressing tumors had significantly reduced disease-free survival in breast cancer. *In vitro*, Cxcl10 induced migration of *ING4*-deleted breast cancer cells but not of *ING4*-intact cells. Using inhibitors, we found that Cxcl10-induced migration of *ING4*-deleted cells required Cxcr3, Egfr, and the G$\beta\gamma$ subunits downstream of Cxcr3 but not Gαi. Immunofluorescent imaging showed that Cxcl10 induced early transient colocalization between Cxcr3 and Egfr in both *ING4*-intact and *ING4*-deleted cells, which recurred only in *ING4*-deleted cells. A peptide agent that binds to the internal juxtamembrane domain of Egfr inhibited Cxcr3/Egfr colocalization and cell migration. Taken together, these results presented a novel mechanism of Cxcl10 that elicits migration of *ING4*-deleted cells, in part by inducing a physical or proximal association between Cxcr3 and Egfr and signaling downstream via G$\beta\gamma$. These results further indicated that ING4 plays a critical role in the regulation of Cxcl10 signaling that enables breast cancer progression.

KEYWORDS CXCL10 chemokine, ING4 tumor suppressor, CXCR3 G protein-coupled receptor, Egfr, breast cancer, cell migration

C-X-C motif chemokine ligand 10 (Cxcl10), also known as Interferon gamma induced protein 10 kDa (IP-10), is a member of the chemokine family secreted by various cell types, including monocytes, T cells, endothelial cells, keratinocytes, and fibroblasts, during normal immune and inflammatory response (1). The main function of Cxcl10 is to mediate chemotactic migration of immune cells expressing the Cxcr3 receptor to the site of inflammation in a concentration gradient-dependent manner (1). Cxcr3 belongs to the large group of the G protein-coupled receptor (GPCR) proteins characterized by their seven transmembrane domains and interaction with the heterotrimeric G$\alpha\beta\gamma$ subunits for downstream signaling (2). Cxcl10-effector immune cells include CD8 cytotoxic T lymphocytes (CTL), CD4 T helper 1 (Th1) cells, and natural killer (NK) cells, whose major function is cytotoxic cell killing (1, 3, 4). As such, excessive Cxcl10 has been implicated in tissue damage related to chronic inflammatory and autoimmune diseases, including rheumatoid arthritis, colitis, and diabetes (5–9).

Cancer cells also express Cxcl10 and/or Cxcr3 (4, 10). Tumor expression of Cxcl10 was initially characterized as a good prognostic indicator correlated with tumor infiltrating lymphocytes (TILs) and therapy response in several cancers, including ovarian, colon, and esophageal cancer (11–16). These observations were concordant with the normal function of Cxcl10 that

Address correspondence to Suwon Kim, suwon@email.arizona.edu.

The authors declare no conflict of interest.

Received 21 September 2021
Returned for modification 12 November 2021
Accepted 1 December 2021
Accepted manuscript posted online 6 December 2021
Published 17 February 2022

elicits immune-mediated cell killing so that Cxcl10 has been utilized as an indicator of robust immune response to therapy in clinical trials (17, 18) and Cxcl10-based cancer therapy has been proposed (19). Antiproliferative effects of Cxcl10 on cells *in vitro* have also been reported, supportive of the anticancer role of Cxcl10 (20, 21). Paradoxically, high expression of Cxcl10 has been correlated with aggressive disease and poor patient survival in several cancers, including breast cancer, pancreatic cancer, and melanoma, suggesting that Cxcl10 may promote cancer progression in some settings (22–25). Consistent with this idea, Cxcl10 increased cell proliferation, migration, and invasion in cell models (26–29). Moreover, Cxcr3 receptor expression in tumors and/or immune cells was shown to be required for tumor metastasis in mouse models (30–35). Collectively, these studies have shown that Cxcl10/Cxcr3 can exert dual opposing effects of tumor killing versus tumor promoting, involving both immune and tumor cells. However, the molecular contexts that allow the switch between the opposing roles of Cxcl10/Cxcr3 are not well understood.

Inhibitor of Growth 4 (ING4) is a tumor suppressor deficient in up to 34% of all breast tumors and correlated with lymph node positivity and poor patient survival (36, 37). ING4 is a member of the plant homeodomain (PHD) containing family that interacts with histone acetylation complexes and regulates gene expression (38–40). We and others have shown that ING4 inhibits NF-κB, a key transcription factor that induces hundreds of genes critical in immune response (36, 41, 42). *CXCL10* was one of the NF-κB target genes repressed by ING4 in breast cancer cells (36), suggesting that ING4 deficiencies may result in upregulation of *CXCL10*. To date, no functional relationship between ING4 and Cxcl10 has been reported. In this study, we investigated the effects of Cxcl10 in the context of ING4 deficiencies, which led to the identification of a novel cross talk mechanism between the Cxcr3 and Egfr receptors that mediated Cxcl10-induced migration of ING4-deficient breast cancer cells.

RESULTS

High *CXCL10* and low *ING4* expression are associated with reduced disease-free survival in breast cancer. Low protein or mRNA expression of ING4 has been correlated with aggressive tumors and poor patient survival in breast cancer (36, 37). Cxcl10 protein expression has been associated with poor prognosis in breast cancer (22), but *CXCL10* gene expression related to patient outcome has not been evaluated elsewhere. To assess potential genetic interactions between *ING4* and *CXCL10*, we analyzed two public gene expression data sets of breast tumors: GDS806 and METABRIC. The GDS806 data set contained gene expression profiles of selective hormone receptor-positive primary tumors ($n = 60$) (49), whereas the METABRIC (Molecular Taxonomy of Breast Cancer International Consortium) data set contained the integrative multiple genomics data of a large cohort of clinically annotated primary tumors ($n = 1903$) collected from multiple tumor banks, representing all molecular subtypes (50, 51).

We first performed Kaplan Meier survival analyses of *ING4* or *CXCL10* individually using the mean expression values as the cutoff. The results showed that patients with low *ING4* expressing tumors had poor disease-free survival in GDS806 (HR = 2.3, 95% CI 1.09 to 4.85, $P = 0.049$ [Fig. 1A]) and in METABRIC (HR 1.16, 95% CI 1.01 to 1.33, $P = 0.043$ [Table 1]), consistent with the previous reports (36, 37). Kaplan Meier analyses for *CXCL10* expression showed that patients with tumors expressing high levels of *CXCL10* had significantly increased rates of recurrence in GDS806 (HR 2.23, 95% CI 1.05 to 4.73, $P = 0.033$ [Fig. 1A]) and in METABRIC (HR 1.24, 95% CI 1.08 to 1.43, $P = 0.003$ [Table 1]). These results were concordant with the previous study showing that Cxcl10 protein expression was associated with poor patient outcomes in breast cancer (22). These results suggested that low *ING4* expression or high *CXCL10* expression may contribute to breast cancer progression independently. We also evaluated *CXCR3* (the Cxcl10 receptor), *CXCL9*, *CXCL11* (two other Cxcr3 ligands), or *EGFR* (epidermal growth factor receptor) for a correlation with patient survival. The results showed that these gene expression levels were not associated with patient survival in the GDS806 data set (Fig. 1C) or in the METABRIC data set (Table 1), highlighting a unique relationship between *ING4* or *CXCL10* expression and aggressive breast cancer.

Next, we evaluated whether *ING4* and *CXCL10* gene expressions together influenced patient survival by using quartile stratification of tumors expressing *ING4*-high/*CXCL10*-high,

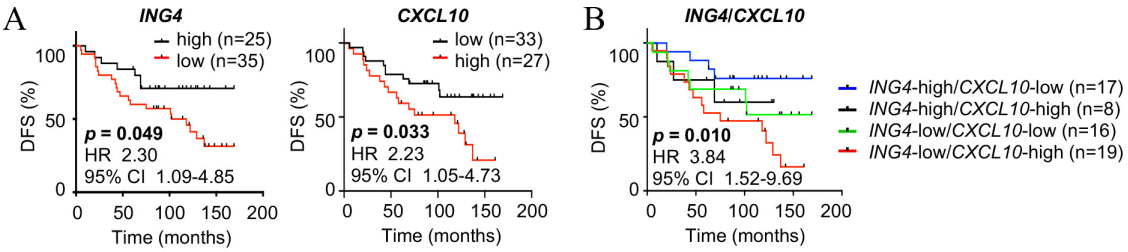

C

Gene	Expression, n		HR	95% CI	p
	Low	High			
CXCL9	35	25	0.98	0.43-2.27	0.971
CXCL11	35	25	2.01	1.96-4.38	0.053
CXCR3	32	28	0.96	0.93-4.14	0.074
EGFR	31	29	1.20	0.57-2.53	0.621

FIG 1 Low *ING4* expression and high *CXCL10* expression correlate with reduced disease-free survival in breast cancer. Kaplan-Meier (KM) analyses of the GDS806 (n = 60) breast tumor gene expression data set. Mean gene expression values were used to stratify tumors. (A and B) Hazard ratio (HR) was determined comparing *ING4*-low to *ING4*-high and *CXCL10*-high to *CXCL10*-low (A) and *ING4*-low/*CXCL10*-high to *ING4*-high/*CXCL10*-low curves (B). (C) KM analyses for *CXCL9*, *CXCL11*, *CXCR3*, and *EGFR* expression. CI, confidence interval; P values were determined by the log rank test and $P < 0.05$ was considered significant.

ING4-high/*CXCL10*-low, *ING4*-low/*CXCL10*-high, or *ING4*-low/*CXCL10*-low. The results showed that *ING4*-low/*CXCL10*-high tumor patients had significantly reduced disease-free survival with a striking 3.84 times the rate of recurrence compared to *ING4*-high/*CXCL10*-low tumor patients in GDS806 (HR 3.84, 95% CI 1.52 to 9.69, P = 0.010 [Fig. 1B]). METABRIC data analysis also showed significantly reduced survival of *ING4*-low/*CXCL10*-high tumor patients compared to *ING4*-high/*CXCL10*-low tumor patients (HR 1.35, 95% CI 1.13 to 1.62, P = 0.001 [Table 2]). The hazard ratios increased for the two gene combination analyses compared to the ones for the *ING4* or *CXCL10* single gene analyses in both GDS806 and METABRIC data sets, suggesting that Cxcl10 may exacerbate the aggressiveness of ING4-deficient tumors or vice versa.

The association between *ING4*-low/*CXCL10*-high expression and patient survival was not significant when tumors were stratified by the molecular subtypes of breast cancer as annotated in the METABRIC data set (Table 2). These results suggested that the effects of Cxcl10 on ING4-deficient tumors may not be specific to a molecular subtype(s) (see Discussion). However, we observed that *ING4*-low/*CXCL10*-high tumors were significantly more prevalent in hormone receptor-negative tumors, compared to hormone receptor-positive tumors: HER2-positive (47.7%), basal (43.2%), and claudin-low (50.3%) subtypes, versus the normal (18.6%), luminal A (16.4%), and luminal B (30.5%) subtypes (red bars in Fig. 2A). Conversely, *ING4*-high/*CXCL10*-low tumors were more prevalent in hormone receptor-positive tumors (blue bars in Fig. 2A). We also analyzed the TCGA (The Cancer Genome Atlas, n = 1,090) data set and found that significantly higher percentages of hormone receptor-negative breast tumors were *ING4*-low/*CXCL10*-high (Fig. 2B). These results suggested

TABLE 1 Kaplan-Meier survival analyses of the METABRIC data set (n = 1,903) for *ING4*, *CXCL10*, *CXCR3*, *CXCL9*, *CXCL11*, and *EGFR*, using the mean gene expression values to stratify patients[a]

	Expression [n (%)]		Disease-free survival			Overall survival		
Gene	Low	High	HR	95% CI	P	HR	95% CI	P
ING4	1,006 (53)	897 (47)	1.16	1.00–1.33	0.043	1.16	1.03–1.30	0.014
CXCL10	971 (51)	932 (49)	1.24	1.08–1.43	0.003	1.13	1.00–1.27	0.045
CXCR3	1,126 (59)	777 (40)	1.10	0.95–1.27	0.176	0.96	0.85–1.08	0.506
CXCL9	1,018 (53)	885 (47)	1.17	1.02–1.35	0.026[b]	1.03	0.91–1.16	0.632[b]
CXCL11	1,258 (66)	645 (34)	1.11	0.96–1.29	0.155	0.99	0.88–1.13	0.920
EGFR	1,269 (67)	634 (33)	1.12	0.96–1.30	0.137	0.94	0.83–1.07	0.338

[a]HR, hazard ratio low to high expression; CI, confidence interval. P values were determined by the log rank (Mantel-Cox) test; $P <$ 0.05 was considered significant.

[b]*CXCL9* showed a significant difference in disease-free survival but not in overall survival.

TABLE 2 Kaplan-Meier disease-free survival analyses of the METABRIC data set for *ING4*-low/*CXCL10*-high versus *ING4*-high/*CXCL10*-low expression in each molecular subtype of breast cancer as annotated in the data set, using the mean gene expression values to stratify patients[a]

	No. (%)				
Subtype	*ING4*-low *CXCL10*-high	*ING4*-high *CXCL10*-low	HR	95% CI	*P*
All	569 (51.6)	534 (48.4)	1.35	1.125–1.621	0.001
Normal	26 (34.7)	49 (65.3)	1.23	0.641−2.369	0.532
Luminal A	111 (30.7)	251 (69.3)	1.42	0.983−2.036	0.058
Luminal B	141 (49.6)	143 (50.4)	1.05	0.746–1.484	0.771
HER2	105 (69.5)	46 (30.5)	1.15	0.714–1.855	0.568
Basal	86 (79.6)	22 (20.4)	1.24	0.698−2.190	0.476
Claudin-low	100 (83.3)	20 (16.7)	1.00	0.524−1.901	0.996

[a]HR, hazard ratio low to high expression; CI, confidence interval. *P* values were determined by the log rank (Mantel-Cox) test; $P < 0.05$ was considered significant.

that *ING4*-low/*CXCL10*-high expression may contribute to the genesis and/or aggressiveness of hormone receptor-negative breast cancers (see Discussion).

Cxcl10 induces migration of *ING4*-deleted, but not of *ING4*-intact, breast cancer cells. As the breast cancer data set analyses showed that *ING4*-low/*CXCL10*-high tumors were more prevalent in hormone receptor-negative breast tumors (Fig. 2), we investigated whether Cxcl10 affected cancer phenotypes of ING4-deficient cells using two triple negative breast cancer (TNBC) cell lines. We engineered the *ING4* gene deletion in MDA-MB-231 and MDA-MB-468 cells utilizing a CRISPR/CAS9 system (43, 44). Four different guide RNA (gRNA) sequences were selected to generate *ING4*-targeting constructs in the v2 CRISPR/CAS9 vector, namely, v2h1, v2h2, v2h3, and v2h4 (see Materials and Methods) (Fig. 3A). We confirmed the *ING4* deletion using Western blot, which showed 87 to 95% reduction of the ING4 protein in v2h1, v2h2, and v2h3 cells, compared to the vector control, v2 (Fig. 3A). V2h4 was excluded from further analysis as ING4 expression was reduced by a nominal 2-fold (Fig. 3A). Variable efficiencies and off-target effects of gRNAs as well as the heterogeneity of gRNA-mediated gene deletions

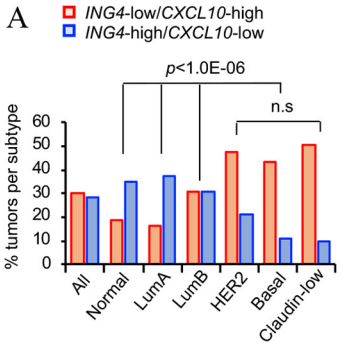

Subtype	Total n	*ING4*-low *CXCL10*-high n (% of total)	*ING4*-high *CXCL10*-low n (% of total)	Fisher's Exact Probability compared to Basal subtype *p*
All	1903	569 (29.9%)	534 (28.1%)	n.d*
Normal	140	26 (18.6%)	49 (35.0%)	<1.0E-06
LumA	677	111 (16.4%)	251 (37.1%)	<1.0E-06
LumB	462	141 (30.5%)	143 (31.0%)	<1.0E-06
HER2	220	105 (47.7%)	46 (20.9%)	0.146
Basal	199	86 (43.2%)	22 (11.1%)	-
Claudin-low	199	100 (50.3%)	20 (10.1%)	0.498

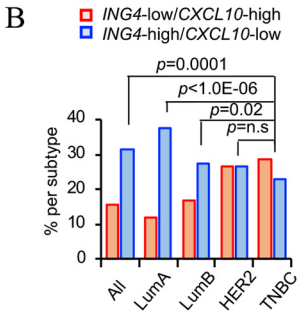

Subtype	Total n	*ING4*-low *CXCL10*-high n (% of total)	*ING4*-high *CXCL10*-low n (% of total)	Fisher's Exact Probability compared to TNBC subtype *p*
All	1090	172 (15.8%)	343 (31.5%)	0.0001
LumA	590	71 (12.0%)	221 (37.5%)	<1.0E-06
LumB	214	36 (16.8%)	59 (27.6%)	0.023
HER2	64	17 (26.6%)	17 (26.6%)	0.684
TNBC	160	46 (28.8%)	37 (23.1%)	-

FIG 2 *ING4*-low/*CXCL10*-high tumors are prevalent in hormone receptor-negative breast cancer. Percentage of tumors with *ING4*-low/*CXCL10*-high or *ING4*-high/*CXCL10*-low expression in all tumors or in the molecular subtypes as annotated in the data set METABRIC (n = 1,903) (A) or TCGA (n = 1,090) (B). Fisher's exact probability test was used to calculate statistical significance of the percent tumor distribution compared to the basal or TNBC subtype; $P < 0.05$ was considered significant. LumA, luminal A; LumB, luminal B; TNBC, triple negative breast cancer; n.s, not significant; n.d*, not determined because of the large sample size not appropriate for Fisher's exact test.

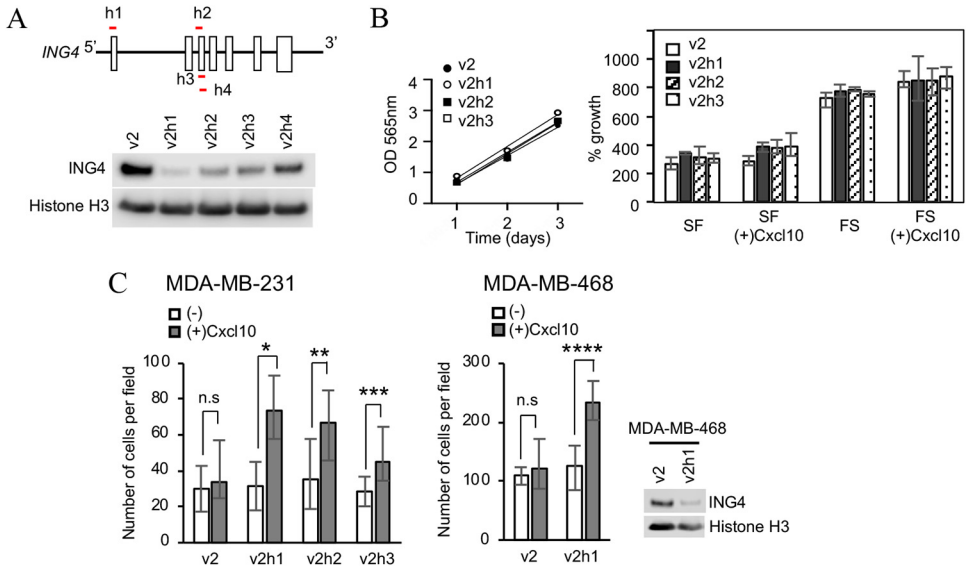

FIG 3 Cxc10 induces migration of *ING4*-deleted breast cancer cells. (A) Schematic diagram of the *ING4* gene (exons are denoted as rectangular boxes) and CRISPR/CAS9 gRNAs h1-h4 (red); Western blot for the ING4 protein in MDA-MB-231 v2 (vector control), v2h1, v2h2, v2h3, and v2h4 cells, using histone H3 as the loading control; (B) MDA-MB-231 cell growth during 3 days in the full serum media (left panel) or in the presence or absence of 10 ng/ml Cxcl10 in the full serum (FS) or serum-free (SF) media (right panel); (C) transwell migration assays with MDA-MB-231 v2, v2h1, v2h2, v2h3 cells (left panel) and MDA-MB-468 v2, v2h1 cells (center panel) in the absence or presence of 10 ng/ml Cxcl10 and Western blot for ING4 in MDA-MB-468 v2 and v2h1 cells, using histone H3 as the loading control (right panel). Number of migrated cells per field was obtained by averaging 6 to 8 field images of each membrane per experiment from at least 3 independent experiments. Statistical significance was determined by an unpaired 2-tailed Student's *t* test. *, $P < 0.0005$; **, $P = 0.005$; ***, $P < 0.05$; ****, $P < 0.00005$.

have been reported previously (52), thus we opted for working with the pools of each gRNA-selected cells rather than clonal populations derived from single gRNA selection.

We evaluated whether *ING4* deletion and/or exogenous Cxcl10 affected cell proliferation using SRB colorimetric assays. The results showed no differences in the growth rates between v2 and *ING4*-deleted v2h1, v2h2, or v2h3 cells (Fig. 3B). Cxcl10 added to the serum free media or full serum media did not alter proliferation of v2, v2h1, v2h2, or v2h3, demonstrating that *ING4* deletion and/or exogenous Cxcl10 did not affect cell proliferation (Fig. 3B).

We next evaluated cell migration, a cancer cell phenotype associated with metastatic potential, using transwell migration assays with or without Cxcl10. The results showed that cell migration in the absence of Cxcl10 was comparable between v2 and *ING4*-deleted cells (v2h1, v2h2, or v2h3) (Fig. 3C, open bars), indicating *ING4* deletion did not affect basal level cell migration. Cxcl10 did not increase migration of v2 cells, but significantly increased migration of v2h1 and v2h2 cells by 2-fold and v2h3 by 1.5-fold in MDA-MB-231 (Fig. 3C, left panel, closed bars). Cxcl10 also increased migration of *ING4*-deleted MDA-MB-468 cells by 2-fold (Fig. 3C, center panel, closed bars). These results demonstrated that Cxcl10 induced migration of *ING4*-deleted cells but not of *ING4*-intact cells, suggesting a synthetic interaction between *ING4*-deletion and Cxcl10.

The Cxcr3 and Egfr receptors are required for Cxcl10-mediated cell migration. We next examined whether Cxcr3, the cognate receptor for Cxcl10, was required for Cxcl10-induced migration of *ING4*-deleted cells by using AMG-487, a competitive inhibitor of Cxcl10 (53). The transwell migration assay results showed that AMG-487 inhibited Cxcl10-induced migration of v2h1 cells (Fig. 4A, 3rd closed bars, amg), indicating that Cxcl10 binding to the Cxcr3 receptor was essential in the cell migratory signal. Unexpectedly, erlotinib, an inhibitor for Egfr (54), also inhibited Cxcl10-induced migration of v2h1 in both MDA-MB-231 and MDA-MB-468 cells (Fig. 4A, 4th closed bars, erl), suggesting that Egfr played a role in Cxcl10-mediated cell migration.

The reason for the use of erlotinib was initially because we asked whether Egf-induced cell migration was also affected in *ING4*-deleted cells, as Egf-induced migration has been well described in the literature (55–57). Transwell migration assays showed that Egf induced

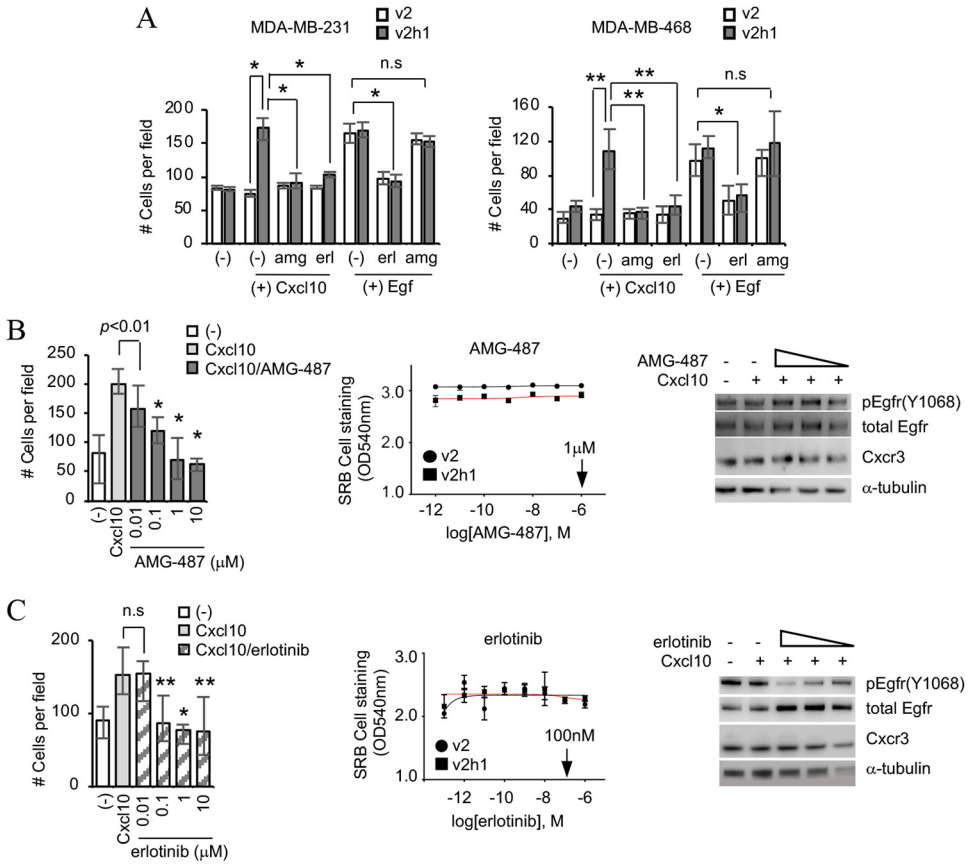

FIG 4 Cxcl10-induced migration of *ING4*-deleted cells is inhibited by a Cxcr3 antagonist or an Egfr inhibitor. (A) Transwell migration assays of v2 (vector) and v2h1 (*ING4* deletion) in the presence of 10 ng/ml Cxcl10 or 10 ng/ml Egf with or without 1 μM AMG-487 (Cxcr3 antagonist; amg) or 100 nM erlotinib (Egfr kinase inhibitor; erl) in MDA-MB-231 (left panel) and MDA-MB-468 (right panel) cells. (-), vehicle; n.s, not significant; *, $P <$ 0.005; **, $P <$ 0.00001. (B) Dose-dependent inhibition of Cxcl10-induced migration of MDA-MB-231 v2h1 cells by AMG-487 (0.01, 0.1, 1, and 10 μM). *, $P <$ 0.0001; IC50 assays with of AMG-487 (1 pM to 1 μM); 1 μM was used from herein (arrow). Western blot showing that AMG-487 (10, 1, 0.1 μM) did not reduce phospho-Egfr (Y1068), total Egfr, or Cxcr3, using α-tubulin as the loading control. (C) Dose-dependent inhibition of Cxcl10-induced migration of MDA-MB-231 v2h1 cells by erlotinib (0.01, 0.1, 1, and 10 μM). *, $P <$ 0.0001; **, $P <$ 0.005; IC50 assays with erlotinib (1 pM to 1 μM); 100 nM was used from herein (arrow). Western blot showing that erlotinib reduced Egfr phosphorylation (Y1068) in a dose-dependent manner (10 μM, 1 μM, and 0.1 μM).

migration of both v2 (*ING4*-intact) and v2h1 (*ING4*-deleted) cells by a comparable 2-fold in both MDA-MB-231 and MDA-MB-468 (Fig. 4A, 5th closed bars), indicating that Egf-induced cell migration was not affected by the *ING4* deletion status. Erlotinib inhibited Egf-induced cell migration as was expected (Fig. 4A, 6th bars, erl). AMG-487, a Cxcr3 antagonist, did not inhibit Egf-induced cell migration (Fig. 3A, 7th bars, amg), indicating that Egf-induced cell migration did not require Cxcr3. These results collectively indicated that unlike Egf-induced cell migration, Cxcl10-induced cell migration was specific to *ING4*-deleted cells and required both the Cxcr3 and Egfr receptors. These results also suggested that Cxcl10 may mediate cell migratory signaling via a potential cross talk between Cxcr3 and Egfr in the absence of ING4.

We evaluated the inhibitory dose of AMG-487 or erlotinib in MDA-MB-231 v2h1 cell migration. The results showed that v2h1 cell migration was inhibited by AMG-487 in a dose-dependent manner (Fig. 4B, closed bars, 0.01 to 10 μM), consistent with the competitive inhibition of Cxcl10 binding to Cxcr3 (53). AMG-487 did not affect cell viability at the concentrations evaluated (Fig. 4B, second graph), indicating that cell migration inhibition was not due to reduced cell viability. Cxcl10 and/or AMG-487 did not affect phosphorylated Egfr (Y1068), total Egfr or Cxcr3 protein levels at 0.1 to 10μM concentration (Fig. 4B, Western blot). Erlotinib inhibited v2h1 cell migration at a concentration of 0.1 μM or higher (Fig. 4C, first graph) without affecting cell viability (Fig. 4C, second graph). Western blot showed

reduction of phosphorylated Egfr at the tyrosine residue 1068 by 90% at 10 μM, 75% at 1 μM, and 20% at 0.1 μM, normalized to tubulin and total Egfr (Fig. 4C, Western blot), confirming that erlotinib inhibited the Egfr kinase activity in a dose-dependent manner. These results indicated that even 20% reduction in the Egfr kinase activity (at 0.1 μM erlotinib) was sufficient to inhibit Cxcl10-induced migration of *ING4*-deleted cells, supportive of the idea that Egfr played a critical role in Cxcl10/Cxcr3 signaling (see Discussion).

Cxcl10 induces recurrent colocalization of Cxcr3 and Egfr in *ING4*-deleted MDA-MB-231 cells. We next explored a potential mechanism for the Cxcr3/Egfr cross talk in Cxcl10 signaling. Studies have shown transactivation of Egfr by G protein-coupled receptors (GPCRs) in cancers (58). In particular, another chemokine receptor, Cxcr7, was shown to associate with Egfr, albeit in a ligand-independent manner (59). Thus, it was plausible that Cxcr3 could directly interact with Egfr in Cxcl10-induced cell migration. To test this, we used immunofluorescent staining for Cxcr3 and Egfr, labeled with red- and green-fluorescent secondary antibodies, respectively, and determine receptor colocalization in the presence or absence of Cxcl10 in *ING4*-intact versus *ING4*-deleted cells. The results showed that the two receptors were not colocalized at steady state in the absence of Cxcl10 in *ING4*-intact (v2) or *ING4*-deleted (v2h1) cells (Fig. 5A; a and e). When cells were treated with Cxcl10, Cxcr3 and Egfr colocalized within 10 min (Fig. 5A; b and f, arrows) in both v2 and v2h1 cells. By 1 h after Cxcl10 treatment, Cxcr3 and Egfr no longer colocalized (Fig. 5A; c and g), indicating that Cxcl10-induced Cxcr3/Egfr association was rapid and transient. Strikingly, the two-receptor colocalization recurred at 24 h after Cxcl10 treatment only in *ING4*-deleted v2h1 cells (Fig. 5A; h) but did not in *ING4*-intact v2 cells (Fig. 5A; d). Higher magnification of the cell images showed that Cxcr3 and Egfr may localize to the different areas of the cell membrane in untreated samples (Fig. 5A; a-l). At 10 min in v2 and v2h1 cells (Fig. 5A; b-l and f-l) and at 24 h in v2h1 cells (Fig. 5A; h-l) after Cxcl10 treatment, Cxcr3 and Egfr colocalized on tail-like protruding portions of the cell membrane. Whether these structures represent filopodia or other membrane structures related to cell migration will require further investigation.

We quantified the pixel intensity of each fluorescence normalized to the pixel intensity of DAPI per image and calculated the mean cell surface expression of Cxcr3 or Egfr. The results showed no significant differences in the expression of Cxcr3 or Egfr between v2 and v2h1 cells treated with or without Cxcl10 at different time points (Fig. 5B).

We determined Manders coefficients (46), a widely used colocalization measurement calculated as the fraction of overlapping fluorescence signals (yellow) in total single color fluorescence signals (red or green) per image (see Materials and Methods). The M1 coefficients, the fraction of Cxcr3 colocalized with Egfr in total Cxcr3 signals (sum of yellow over sum of red), are presented in a Dot Plot with each dot representing the M1 value per image (Fig. 5C). The resulted showed that the mean M1 values increased significantly from 0 to 0.4 to 0.6, at 10 min after Cxcl10 treatment in both v2 and v2h1 cells and at 24 h after Cxcl10 treatment in v2h1 cells only (Fig. 5C). These calculations substantiated the visual observations that the two receptors colocalized at 10 min after Cxcl10 treatment in both *ING4*-intact and *ING4*-deleted cells, which dissociated by 1 h despite the continuous presence of Cxcl10, and that the receptor colocalization recurred in *ING4*-deleted cells, but not in *ING4*-intact cells, by 24 h after Cxcl10 treatment (Fig. 5C).

Western blot analysis showed that v2 and v2h1 cells expressed comparable amounts of receptor proteins at the time points chosen for immunofluorescent staining (Fig. 5D), consistent with the immunofluorescent pixel density quantification in Fig. 5B Autophosphorylation of Egfr at the amino acid residue Y1068 did not vary after Cxcl10 treatment at any time points (Fig. 5D). Of note, two alterative spliced isoforms of Cxcr3, Cxcr3B (larger band) and Cxcr3A (smaller band) (3), were expressed and comparable between v2 versus v2h1 cells, indicating that *ING4* deletion or Cxcl10 treatment did not alter the Cxcr3 protein or isoform expression (Fig. 5D). These results showed that no drastic changes in the receptor proteins occurred at the receptor colocalization time points.

We also evaluated the recurrent receptor colocalization in v2h2 and v2h3 cells (*ING4*-deleted cells using h2 and h3 CRISPR gRNA sequence constructs [Fig. 3A]). The results showed the receptor colocalization (Fig. 5E) with significant increases in the M1 coefficients at 10 min and at 24 h after Cxcl10 treatment in both v2h2 and v2h3 cells (Fig. 5F), as did in v2h1 cells.

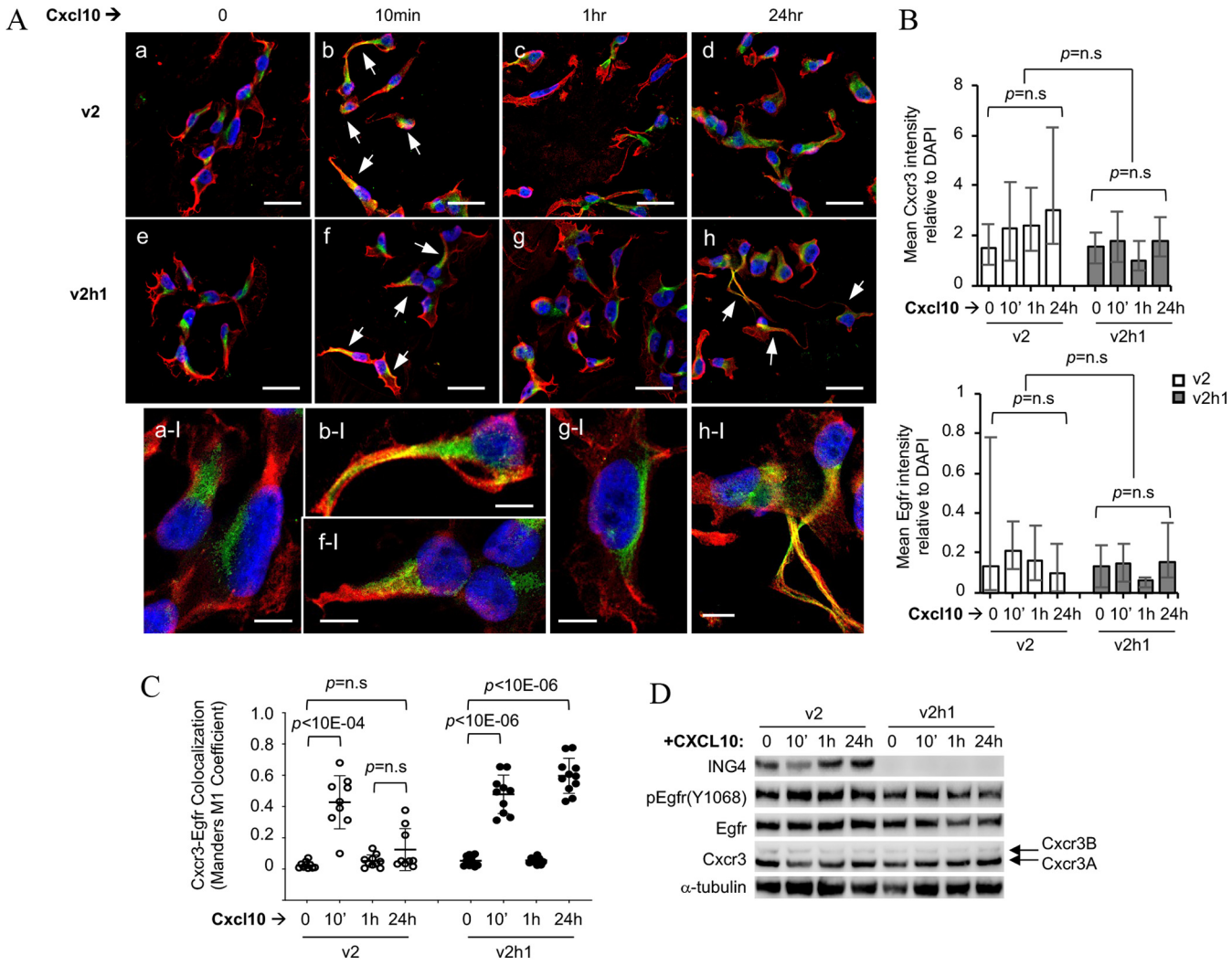

FIG 5a

Taken together, we concluded that Cxcl10 induced early transient association between Cxcr3 and Egfr in MDA-MB-231 cells, which recurred at a later time only in *ING4*-deleted cells.

Recurrent colocalization of Cxcr3/Egfr in *ING4*-deleted MDA-MB-468 cells. We next examined whether Cxcl10-induced Cxcr3/Egfr colocalization also occurred in MDA-MB-468 v2 and v2h1 cells. Immunostaining showed that the membrane compartmentalization of Cxcr3 and Egfr was more pronounced in MDA-MB-468 cells compared to MDA-MB-231 cells; Egfr was predominantly localized to the membrane portions bordering neighboring cells, whereas Cxcr3 was localized to the membrane portions not in contact with the neighboring cells in untreated cells (Fig. 6A; a, f, and f inset). As was in MDA-MB-231 cells, the receptor colocalization was observed at 10 min after Cxcl10 treatment in both v2 and v2h1 cells (Fig. 6A; b and g), which disappeared by 1 h after Cxcl10 treatment (Fig. 6A; c and h) in MDA-MB-468 cells. However, we did not observe the recurrent colocalization of Cxcr3/Egfr at 24 h after Cxcl10 treatment in MDA-MB-468 v2h1 cells (Fig. 6A; d and i). We postulated that MDA-MB-468 cells may have a delayed timeline for Cxcr3/Egfr colocalization recurrence as these cells grew much slower with a doubling time of 41 h (60), compared to MDA-MB-231 cells with a considerably shorter doubling time of 27 h (61). We extended the time point and observed the recurrent colocalization of Cxcr3/Egfr at 48 h after Cxcl10 treatment only in *ING4*-deleted MDA-MB-468 cells (Fig. 6A; e versus j). The cell surface expression of Cxcr3 or Egfr reflected in the pixel intensity measurements did not vary significantly between the time points of Cxcl10 treatment (Fig. 6B). Manders M1 coefficient calculations showed a significant increase in colocalization at 10 min in both v2 and v2h1 cells, while the receptor colocalization recurred at 48 h

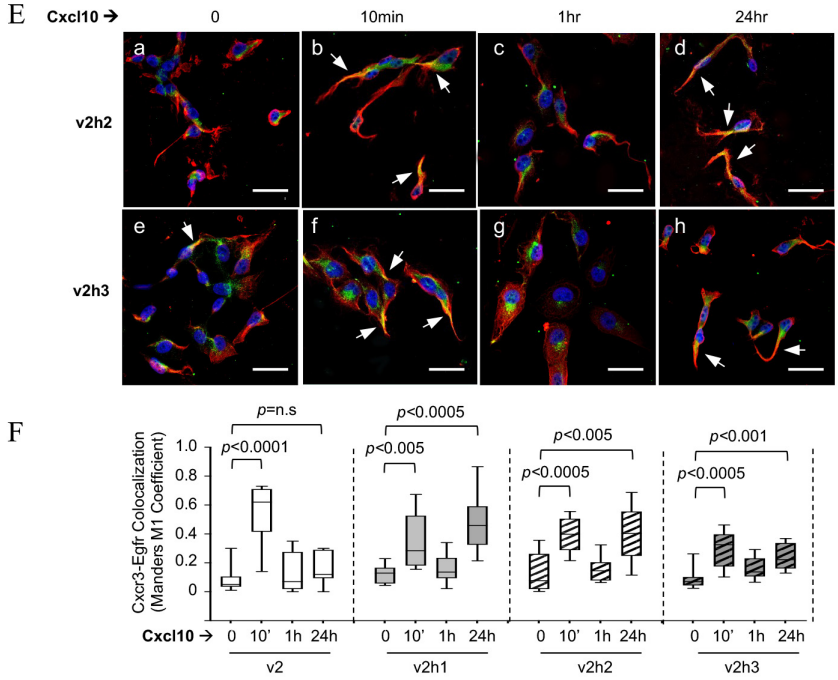

FIG 5 Cxcl10 induces early transient colocalization of Cxcr3 and Egfr, which recurs only in *ING4*-deleted MDA-MB-231 cells. (A) Immunofluorescent staining of v2 (vector [a to d]) and v2h1 (*ING4* deletion [f to h]) cells treated with 10 ng/ml Cxcl10 for 0, 10 min, 1 h, and 24 h. Higher magnification images selected from panels a, b, f, g, and h, are shown (a-l, b-l, f-l, g-l, h-l). Cxcr3 (red), Egfr (green), and 4′,6-diamidino-2-phenylindole (DAPI, blue); arrows indicate colocalization (yellow); scale bars represent 40 μm (a to h) and 10 μm (a-l, b-l, f-l, g-l, and h-l). (B) Quantification of the pixel intensity for Cxcr3 (top panel) and Egfr (bottom panel) relative to DAPI. (C) Quantification of Cxcr3/Egfr colocalization using Manders M1 coefficient calculations presented in a dot plot. Each dot represents the M1 value of an image. A minimum 8 images per condition were obtained per experiment and each experiment was repeated at least 3 times. Error bars represent the standard deviation of the mean M1 value. *P* values were determined by an unpaired Student's *t* test; n.s, not significant. (D) Western blot of Cxcl10-treated cells for ING4, pEgfr, Egfr, and Cxcr3, using α-tubulin as the loading control. (E) Immunofluorescent staining of v2h2 (*ING4* deletion with CRISPR gRNA h2 [Fig. 2A]) and v2h3 (*ING4* deletion using CRISPR gRNA h3 [Fig. 2A]) MDA-MB-231 cells treated with 10 ng/ml Cxcl10 for 0, 10 min, 1 h, and 24 h; Cxcr3 (red), Egfr (green), and DAPI (blue); arrows indicate colocalization (yellow); scale bars represent 40 μm. (F) Quantification of Cxcr3/Egfr colocalization using Manders M1 coefficient calculations compared to the M1 values of v2 and v2h1 immunostaining in a box plot with the median values. The error bars denote maximum and minimum M1 values. Statistical significance was determined by an unpaired Student's *t* test; $P < 0.01$ was considered significant.

after Cxcl10 treatment only in v2h1 cells (Fig. 6C). These results do not suggest that the Cxcr3/Egfr colocalization is related to the cell cycle, but hint at temporal variations of the recurrent receptor colocalization in different cell lines. Future mapping of the detailed colocalization timeline may provide insight. Nevertheless, the recurrent colocalization of Cxcr3/Egfr in MDA-MB-468 v2h1 cells provided supporting evidence that Cxcl10-induced Cxcr3/Egfr colocalization recurred specifically in ING4-deficient breast cancer cells.

Cxcl10-induced Cxcr3/Egfr colocalization requires Cxcl10 binding to Cxcr3 and the juxtamembrane domain of Egfr but not the Egfr kinase activity. As Cxcl10-induced migration of *ING4*-deleted cells was inhibited by AMG-487 or erlotinib (Fig. 3), we investigated whether these inhibitors affected Cxcl10-induced Cxcr3/Egfr colocalization. Immunofluorescent staining of cells treated with Cxcl10 in the presence of inhibitors showed that Cxcl10-induced receptor colocalization was inhibited by AMG-487 (Fig. 7A; and c and g), but not by erlotinib (Fig. 7A; d and h) at 10 min in both v2 and v2h1. Manders coefficient calculations confirmed the significant inhibition of the receptor colocalization by AMG-487 (Fig. 7B). As AMG-487 is a competitive inhibitor of Cxcl10 (53), these results suggested that a Cxcl10 binding-induced conformation change(s) of Cxcr3 may be critical for Cxcr3/Egfr association and cell migration. In contrast, erlotinib, an Egfr kinase inhibitor, had no effect on Cxcl10-induced Cxcr3/Egfr colocalization, indicating that the Egfr kinase activity was not required for the receptor association, but required for cell migration.

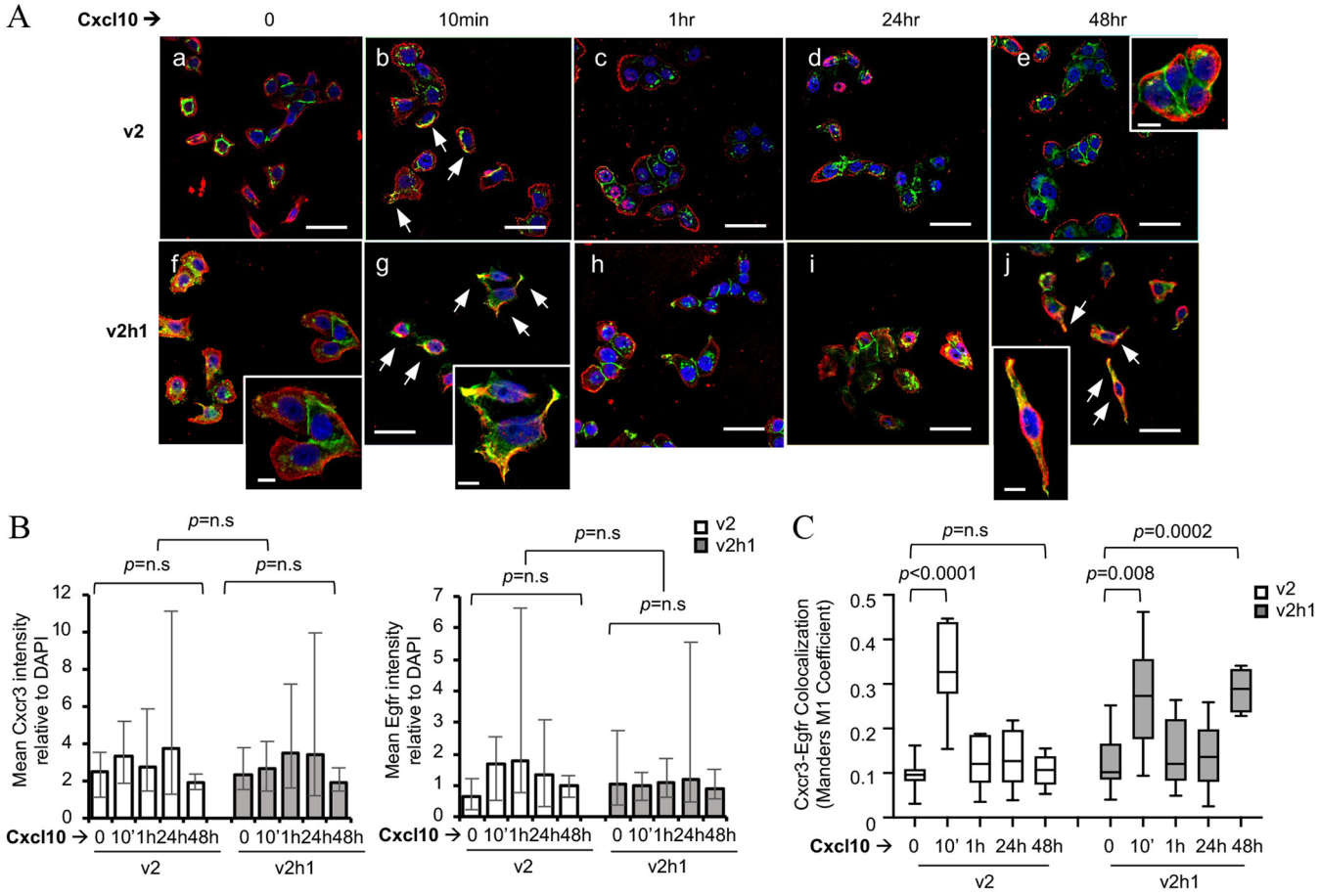

FIG 6 Cxcl10-induced colocalization of Cxcr3 and Egfr recurs in *ING4*-deleted cells in another triple negative breast cancer cell line, MDA-MB-468. (A) Immunofluorescent staining of v2 (vector [a to e]) and v2h1 (*ING4*-deletion [f to j]) cells treated with 10 ng/ml Cxcl10 for 0, 10 min, 1 h, 24 h, and 48 h. Red, Cxcr3; green, Egfr; blue, DAPI; arrows indicate colocalization (yellow); scale bars represent 40 μm (a to j) and 10 μm (insets). (B) Quantification of the pixel intensity of Cxcr3 (left panel) and Egfr (right panel) relative to DAPI. (C) Box plot of the Manders M1 coefficient values representing Cxcr3/Egfr colocalization. *P* values were determined using an unpaired Student's *t* test; $P < 0.01$ was considered significant; n.s, not significant.

To evaluate whether another mode of Egfr inhibition would disrupt the Cxcl10-induced Cxcr3/Egfr cross talk, we used SAH-EJ1, a peptide agent that mimics the juxtamembrane domain of Egfr, thereby inhibiting Egfr (62). The results showed that SAH-EJ1 inhibited Cxcl10-induced Cxcr3/Egfr colocalization (Fig. 7C; f), while the SAH-control peptide had no effect (Fig. 7C; e). Manders M1 coefficient calculations confirmed that AMG-487 and SAH-EJ1 significantly inhibited Cxcr3/Egfr colocalization, compared to Cxcl10-treated and SAH-control peptide treated cells, respectively, whereas there was no difference in colocalization between Cxcl10-treated cells and Cxcl10/erlotinib-treated cells (Fig. 7D). These results indicated that the juxtamembrane domain of Egfr played a major role in Cxcl10-induced two-receptor association, potentially with SAH-EJ1 exerting a steric and/or conformational hindrance.

SAH-EJ1 inhibited Cxcl10-induced cell migration in a dose dependent manner (Fig. 7E, dark gray bars at 1 μM and 10 μM) without affecting cell viability (Fig. 7E, right graph). The inhibition of cell migration by 1 μM SAH-EJ1 was comparable to the inhibition by 1 μM AMG-487 or 100 nM erlotinib (Fig. 7F). Western blotting showed that the Cxcr3 or Egfr protein amounts were comparable between cells treated with or without the inhibitors, indicating that the inhibitors did not affect protein expression or degradation (Fig. 7G). Erlotinib at 100 nM decreased amounts of phosphorylated Egfr at Y1068 by 20 to 40% (Fig. 7G) as was shown in Fig. 4C.

In summary, these results indicated that Cxcl10 binding to Cxcr3 and the juxtamembrane domain of Egfr played a critical role in the Cxcr3/Egfr receptor association and cell migration. In contrast, the Egfr kinase activity was required for cell migration but not for

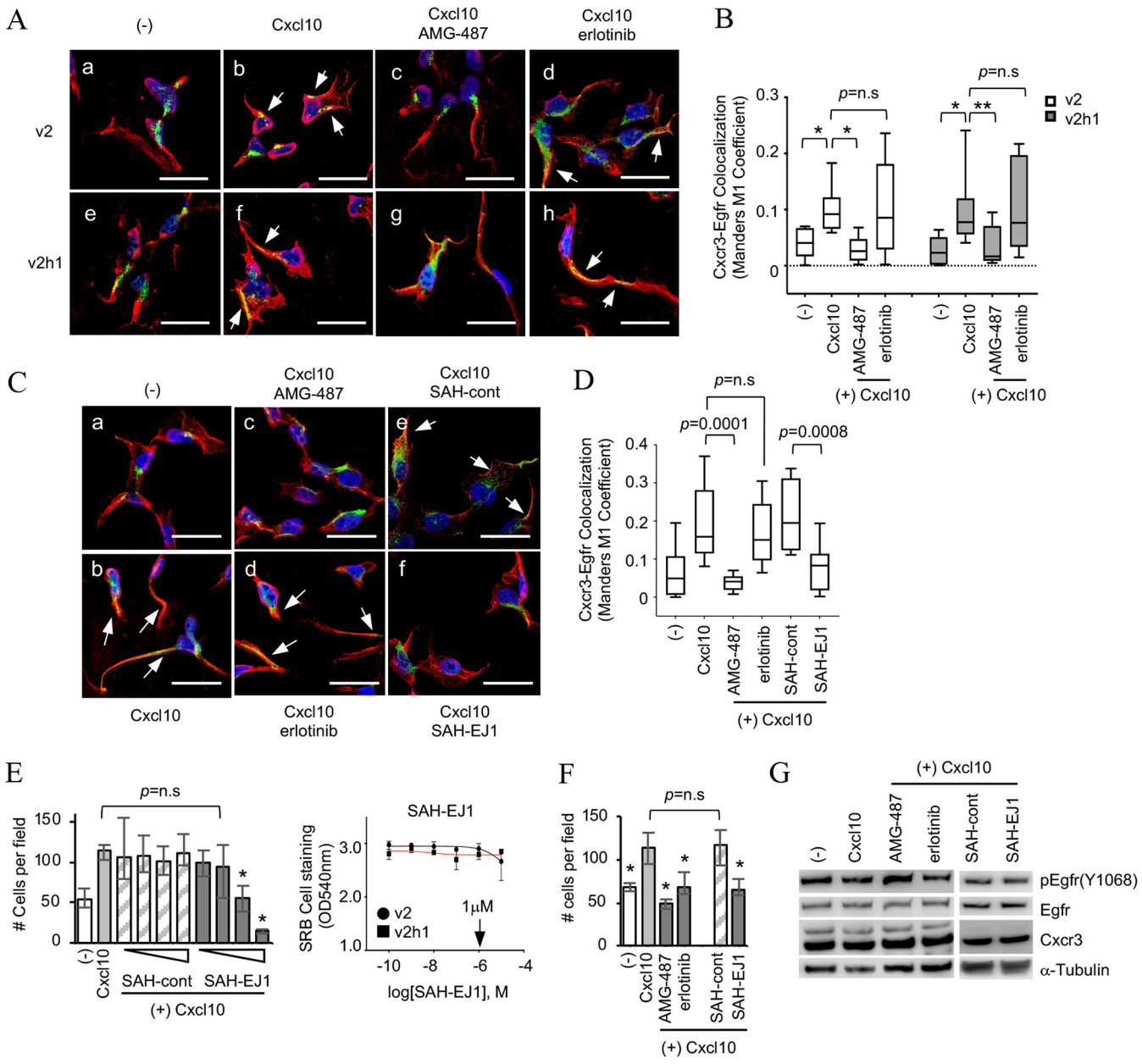

FIG 7 Cxcl10-induced Cxcr3/Egfr colocalization is inhibited by AMG-487 or SAH-EJ1 but not by erlotinib. (A) Immunostaining of MDA-MB-231 *ING4*-intact (v2 [a to d]) and *ING4*-deleted (v2h1 [e to h]) cells treated with (b to d and f to h) or without (a and e) Cxcl10 for 10 min in the presence of 1 μM AMG-487 (c, g) or 100 nM erlotinib (d, h). Red, Cxcr3; green, Egfr; blue, DAPI; scale bars represent 40 μm; arrows indicate Cxcr3/Egfr colocalization resulting in yellow fluorescent signals. (B) Manders M1 coefficients of the images in panel A. M1 values were calculated per image and collected at least 8 images per condition and presented in a box plot with the median values and error bars representing the minimum and maximum values. *, $P < 0.005$; **, $P < 0.05$; n.s, not significant. (C) Immunofluorescent staining of v2h1 (*ING4* deletion) cells treated with (b to f) or without (a) 10 ng/ml Cxcl10 for 24 h in the presence of inhibitors: 1 μM AMG-487 (c), 100 nM erlotinib (d), 1 μM SAH-cont (e), 1 μM SAH-EJ1 (f). Red, Cxcr3; green, Egfr; blue, DAPI; arrows indicate colocalization (yellow); scale bars represent 40 μm. (D) Quantification of Cxcr3/Egfr colocalization using Manders M1 coefficient calculation. M1 values obtained from 10 to 12 images were presented in a box plot; (-), no treatment; SAH-cont, SAH-control peptide; *P* values were determined by an unpaired Student's *t* test and $P < 0.01$ was considered significant; n.s, not significant. (E) Dose-dependent Cxcl10-induced migration by SAH-EJ1. In transwell migration assays, v2h1 cells were treated with vehicle (-) or 10 ng/ml Cxcl10 in the presence of SAH-control peptide (0.01, 0.1, 1, 10 μM) or SAH-EJ1 (0.01, 0.1, 1, 10 μM). *, $P < 1.0E{-}6$ (F) Inhibition of v2h1 cell migration by 1 μM SAH-EJ1 compared to the inhibition by 1 μM AMG-487 or 100 nM erlotinib. *, $P < 0.001$. (G) Western blot of v2h1 cells treated with Cxcl10 or Cxcl10/inhibitor for 24 h for pEgfr, Egfr, and Cxcr3, using α-tubulin as the loading control.

the receptor association, suggesting that Egfr kinase may act downstream of the Cxcr3/Egfr colocalization for cell migration.

G$\beta\gamma$ subunits downstream of the Cxcr3 are required for Cxcl10-mediated migration of *ING4*-deleted cells. We next investigated whether the heterotrimeric G subunits downstream of Cxcr3 affected Cxcl10-induced cell migration and/or Cxcr3/Egfr colocalization. Cxcr3

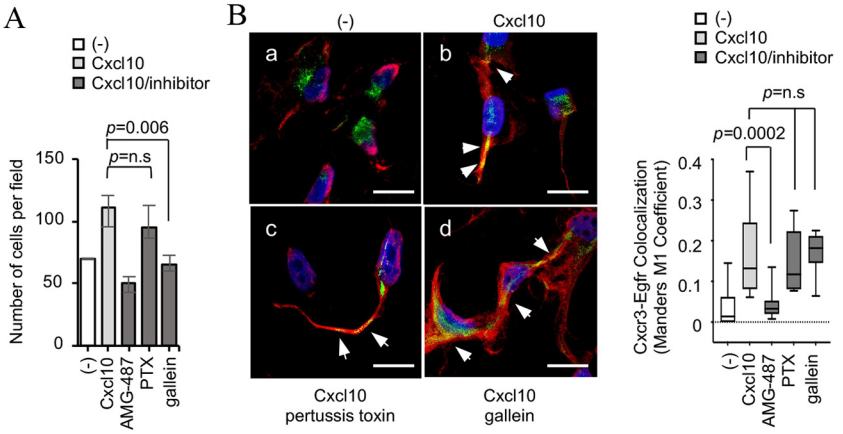

FIG 8 Cxcl10/Cxcr3-mediated migration of *ING4*-deleted cells requires the heterotrimeric G$\beta\gamma$ subunits, but not Gαi. (A) Transwell migration assays with MDA-MB-231 v2h1 (*ING4* deletion) cells with or without 10 ng/ml Cxcl10 in the presence of inhibitors: 1 μM AMG-487, 100 ng/ml pertussis toxin (PTX, a Gαi inhibitor), 10 μM gallein (a G$\beta\gamma$ inhibitor). (B) Immunofluorescent staining of MDA-MB-231 v2h1 cells treated with (a) or without (b to d) 10 ng/ml Cxcl10 for 24 h in the presence of 100 ng/ml PTX (c) or 10 μM gallein (d). Red, Cxcr3; green, Egfr; blue, DAPI; arrowheads indicate colocalization (yellow); scale bars represent 20 μm; quantification of colocalization using Manders M1 coefficient calculation. M1 values obtained from a minimum 10 images per condition are presented in a box plot; $P < 0.01$ determined by an unpaired Student's *t* test was considered significant; (-), no treatment; n.s, not significant.

is one of the GPCRs that signal through the heterotrimeric G-protein subunits, Gαi and G$\beta\gamma$ (63, 64). We evaluated whether Gαi and/or G$\beta\gamma$ were required for Cxcl10/Cxcr3-mediated migration and/or Cxcr3/Egfr colocalization by using inhibitors, pertussis toxin (Gαi inhibitor) and gallein (G$\beta\gamma$ inhibitor) (65, 66). Transwell migration assays showed Cxcl10-induced migration was inhibited by gallein, but not by pertussis toxin (Fig. 8A), indicating G$\beta\gamma$ as a downstream component of Cxcl10/Cxcr3 signaling for cell migration. Neither gallein nor pertussis toxin inhibited Cxcl10-induced Cxcr3/Egfr colocalization (Fig. 7B, c to d). Manders coefficient calculations confirmed no significant changes in Cxcr3/Egfr colocalization in cells treated with gallein or pertussis toxin (Fig. 8B graph). These results suggested that G$\beta\gamma$ may be downstream of the Cxcr3/Egfr receptor colocalization in the Cxcl10-induced migratory signal pathway.

Taken together, we present a working model of Cxcl10-induced migration of *ING4*-deleted breast cancer cells (Fig. 9). In this model, (i) Cxcr3 and Egfr are not associated with each other in the absence of Cxcl10, (ii) Cxcl10 binding to Cxcr3 induces a conformational change in Cxcr3, which allows Cxcr3 to associate with Egfr, (iii) the Cxcl10/Cxcr3/Egfr complex activates Egfr kinase and the G$\beta\gamma$ subunits simultaneously or sequentially to engage a downstream component(s) that relays a "cell migratory" signal to the nucleus, (iv) ING4 in the nucleus inhibits the signal, and (v) in the absence of ING4, the signal leads to recurrent Cxcr3/Egfr colocalization/signaling that mediates cell migration (see Discussion).

DISCUSSION

In this study, we presented evidence for an inverse functional relationship between the ING4 tumor suppressor and the Cxcl10 chemokine in breast cancer. In this setting,

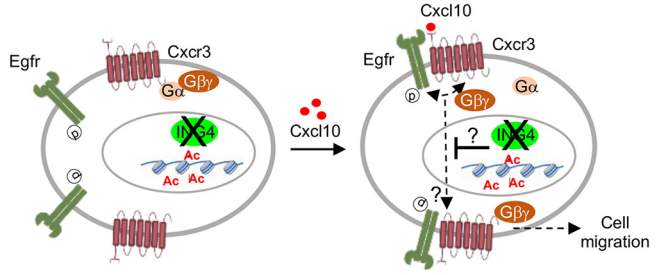

FIG 9 A working model of Cxcl10 signaling in ING4-deficient breast cancer cell migration.

Cxcl10 may exert an oncogenic effect on ING4-deficient tumors, contributing to aggressive breast cancer. Clinical relevance of *ING4*-low/*CXCL10*-high breast cancer was indicated by our patient survival analyses using public gene expression data sets showing significant association with poor patient outcomes.

Genomic data sets provide invaluable resources for correlation studies to evaluate expression of a gene(s) across multiple tumors, but are variable depending on the cohort size, tumor selection, clinical annotation, and technology platform among many others. The gene expression data sets used in this study may illustrate such a diversity in the data sets. The GDS806 data set consists of a selected small cohort of 60 hormone receptor-positive primary tumors from patients who remained disease-free or relapsed during a 15-year follow up. As the tumor samples between the disease-free and relapsed patient groups were matched for clinical profiles and histopathologic tumor characteristics, GDS806 offered a fine-tuned data set that could be used to compare gene expressions and patient survival without adjusting for other compounding factors. METABRIC on the other hand, contains the genomics data from a large cohort of ~2,000 primary breast tumors collected from multiple tumor banks without preset criteria, representing population-based tumor subtype distributions. The large cohort size provided statistical power, but the correlation may be blunted in part due to compounding variables. These may in part explain why the significant association between *ING4*-low/*CXCL10*-high expression and poor patient survival found in all tumors was not observed when tumors were separated by the molecular subtypes. Although we suggested in the text that the genetic interaction between *ING4* and *CXCL10* may not be specific to any molecular subtype(s), it is also possible that the other factors (e.g., tumor grade, patient age, or lymph node status) may have influenced the correlative analysis outcomes within each molecular subtype group. Multivariate analyses and/or selecting a "matched" tumor cohort to ask a specific correlation between two genes may address this possibility and are part of our ongoing investigation.

Intriguingly, *ING4*-low/*CXCL10*-high tumors were significantly more prevalent in the molecular subtypes that were hormone receptor-negative tumors. The exact causal relationship between *ING4*/*CXCL10* expression and the hormone receptor status is unclear. Since ING4 inhibits NF-κB (36, 41, 42, 67), ING4-deficient tumors are likely to have aberrantly activated NF-κB in an inflammatory microenvironment, resulting in high expression of *CXCL10*. This could explain the prevalence of *ING4*-low/*CXCL10*-high tumors in hormone receptor-negative breast cancers that are often associated with the inflammatory/immune gene signatures (68). Elevated expression of Cxcl10 may in turn induce migration of ING4-deficient tumor cells in an autocrine manner. Increased cell migration *in vitro* often indicates aggressive cancer phenotype and increased metastatic potential. Although poor patient survival associated with *ING4*-low/*CXCL10*-high tumors is also consistent with the idea of high metastatic potential, whether Cxcl10 directly promotes metastasis of *ING4*-deficient tumors needs to be evaluated *in vivo* and is part of our ongoing investigation.

In the pursuit of Cxcl10 signaling in ING4-deficient cells, we uncovered a cross talk between Cxcr3 and Egfr, which elicits many more mechanistic questions that are currently unclear. Our study showed that Cxcl10-induced Cxcr3/Egfr colocalization was rapid and transient in both *ING4*-intact and *ING4*-deleted cells. How do these two receptors associate and dissociate? Our current hypothesis is that Cxcl10 binding to Cxcr3 results in a conformational change in the receptor Cxcr3, exposing a domain that can physically interact with Egfr. The results that the Egfr juxtamembrane domain peptide agent inhibited the two-receptor association may support the idea of a direct interaction between the receptors. In this setting, Cxcl10 ligand dissociating from Cxcr3 would rapidly reverse the two-receptor interactions. Both ligand-bound Egfr and GPCRs have independently been shown to recycle via endocytosis pathways where the ligands are removed from the receptor (2, 69). It is possible that the Cxcr3/Egfr complex are endocytosed after Cxcl10-induced association and recycled without Cxcl10 in the conformations not favorable for the receptor interaction. However, our experiments were conducted in the continuous presence of Cxcl10 so that even if the ligand/receptors dissociated upon recycling, Cxcl10 binding would have induced

reassociation regardless of the *ING4* deletion status. But this was not the case, suggesting a different mechanism for receptor dissociation/reassociation.

The mechanism of Cxcl10/Cxcr3 signaling would be unquestionably more complex than as presented in this study. The cross talk mechanism between other GPCRs and Egfr has been reported with Grk, Src, or β-arrestin as the signaling intermediaries between the receptors (58). Whether Cxcl10-induced Cxcr3/Egfr cross talk also requires these "adaptor" molecules needs further investigation. Moreover, since the Egfr kinase activity was also required for the Cxcr3/Egfr cross talk in migration of ING4-deficient cells, it would be important to identify the Egfr kinase substrate(s) in this signaling mechanism. The immediate substrate candidates may include Cxcr3 and/or G$\beta\gamma$. It is also possible that Egfr phosphorylates the Gα subunit, thereby releasing G$\beta\gamma$ from the inactive G$\alpha\beta\gamma$ complex. We are currently investigating these possibilites.

Previous studies have shown that G$\beta\gamma$ plays a critical role in breast cancer cell migration or metastasis mediated by GPCRs, including Cxcr4 and LPA receptors (70, 71). There are consistent with our findings that Cxcl10/Cxcr3 signaling requires G$\beta\gamma$. However, the previous studies showed that Gα was also required in the GPCR-induced cell migration, whereas Cxcl10/Cxcr3-induced cell migration in our study was not affected by a Gα inhibitor. These may attest to the diverse signaling pathway network of GPCRs with similarities and differences in their signaling components. We have not tested whether other GPCRs (Cxcl12/Cxcr4, for example) induce migration of *ING4*-deleted cells. These lines of future investigation may provide insight into the role of ING4 in the regulation of GPCR signaling. The mechanism of ING4 in the inhibition of Cxc10/Cxcr3 signaling is presently unclear. Considering that ING4 is a transcriptional regulator, it is postulated that ING4 regulates expression of a gene(s) critical in the signaling relay from Cxcl10/Cxcr3 to the cell migratory machinery. We are currently pursuing RNAseq to identify relevant genes differentially expressed in *ING4*-deleted cells.

Lastly, we have characterized the Cxcr3/Egfr cross talk in two triple-negative breast cancer cell lines in this study. However, since *ING4*-low/*CXCL10*-high expression was associated with poor patient outcomes in all tumor types, it is possible that Cxcl10/Cxcr3 interacts with other Egfr family members such as the Her2/neu receptor overexpressed in the HER2 molecular subtype (72). We are currently investigating whether Cxcr3 and Her2 interact in the context of ING4-deficient cells. Likewise, a large percentage of glioma and non-small cell lung carcinomas also express Egfr (73, 74). As *ING4* is frequently deleted or downregulated in these cancer types (42, 75, 76), it would be of interest to evaluate the Cxcl10/Cxcr3/Egfr cross talk in the context of ING4-deficiencies, which may have a broader implication with regard to diagnostic markers and therapy targets.

In summary, we have demonstrated that Cxcl10 contributes to aggressive breast cancer in part by inducing migration in cancer cells specifically deficient in the ING4 tumor suppressor. Cxcl10 signaling required Cxcl10 binding to Cxcr3, which induced the receptor cross talk between Cxcr3 and Egfr, resulting in a signal relay via G$\beta\gamma$ to mediate cell migration. These results present a novel signaling pathway of Cxcl10/Cxcr3/Egfr/G$\beta\gamma$ regulated by ING4 and suggest that targeting the Cxcl10/Cxcr3/Egfr/G$\beta\gamma$ axis may have a potential therapeutic benefit in ING4-deficient breast cancer.

MATERIALS AND METHODS

Cell Lines and CRISPR/CAS9-mediated gene deletion. MDA-MB-231 and MDA-MB-468 breast cancer cells were obtained from the American Type Culture Collection (ATCC, Manassas, VA) and cultured in Dulbecco's modified Eagle medium (DMEM) supplemented with 10% fetal bovine serum (FBS) and 1× MEM nonessential amino acids solution (Thermo Fisher Scientific, Waltham, MA). For the CRISPR/CAS9-mediated *ING4* gene deletion constructs, four guide RNA (gRNA) sequences targeting *ING4* were selected using the Zhang lab CAS9 target design tools and protocol (43, 44). The sequences were as follows: h1, 5′-GATGGCTGC GGGGATGTATT; h2, 5′-CTGAGTATATGAGTAGTGCC; h3, 5′-GAGCTCCGAGGAAAAATTGG; and h4, 5′-GGCCCTTC TCAAACAGATCC. Custom-made oligonucleotides (Thermo Fisher Scientific) were cloned into the lentiCRISPRv2 plasmid, referred as "v2" herein, purchased from Addgene (Watertown, MA), constructing v2h1, v2h2, v2h3, and v2h4. Lentiviral particles were produced by cotransfecting v2 constructs with the viral packaging plasmids, pVSVg and psPAX2, (Addgene), into HEK293 (F)T cells (ATCC) using Effectene transfection agent (Qiagen, Germantown, MD). The media containing viral particles were filtered through 0.4 μm syringe filter (Fisher Scientific, Pittsburg, PA) and used to infect cells in the presence of 1 μg/ml Polybrene (Sigma-Aldrich, St. Louis,

MO). Cells transduced with the viral particles were selected in the media containing 2 μg/ml puromycin (Sigma-Aldrich) for 10 to 14 days.

Western blot antibodies. Cell lysate fractionation and Western blot were performed as previously described (36). Antibodies were used against ING4 (BTIM-4 clone, 1:4 [36]; MABE1156, MilliporeSigma, Burlington, MA), Cxcr3 (MAB-160, 1:1000, R&D Systems, Minneapolis, MN), Egfr (rabbit polyclonal number 2232, 1:1000, Cell Signaling Technology [CST], Danvers, MA), pEgfr (D7A5 rabbit monoclonal, 1:1000, CST), histone H3 (1:5000, CST), and α-tubulin (1:5000, Sigma-Aldrich). HRP-conjugated anti-mouse and anti-rabbit secondary antibodies were used (1:5000, Thermo Fisher Scientific) and detected using Immobilon ECL Ultra Western HRP Substrate reagents (MilliporeSigma). Western blot images were acquired and analyzed using the LI-COR Odyssey Fc Imaging System and the LI-COR software Image Studio Lite (LI-COR Biosciences, Lincoln, NE).

Cell proliferation and migration assays. Cell proliferation assays were performed using sulforhodamine B (SRB) staining as described previously (45). Cell migration assays were performed using transwell inserts as described previously (36). In brief, 50,000 cells were placed in inserts containing a semipermeable membrane with 8 μm-sized pores (Fisher Scientific). Recombinant human Cxcl10 (R&D Systems) or EGF (Invitrogen, Carlsbad, CA) was dissolved in PBS containing 0.1% bovine serum albumin (BSA, Sigma-Aldrich). Inhibitors were dissolved in dimethyl sulfoxide (DMSO, Fisher Scientific): AMG-487 (R&D Systems), erlotinib (Selleck Chemicals, Houston, TX), pertussis toxin (Tocris Bioscience, Bristol, UK), and gallein (Tocris Bioscience). Cells on the membrane in the inset chamber were removed using a cotton swab and cells on the bottom side of the membrane were fixed using 100% cold methanol (Fisher Scientific). Fixed cells were stained with 4′,6-diamidino-2-phenylindole (DAPI; Vector Labs, Burlingame, CA) and visualized under a fluorescence microscope. Cell numbers were determined by averaging cell counts from a minimum of 6 field images per membrane.

Immunofluorescent Staining. Cells were plated on 8-well culture slides (Corning Inc, Corning, NY) in the full-serum media overnight and treated next day with various agents in the serum-free media. Treated cells were then fixed with 4% paraformaldehyde (Ted Pella, Inc, Redding, CA) for 20 min, permeabilized with PBS containing 0.2% Triton X-100 (Sigma-Aldrich) for 5 min, and blocked with 0.2% fish skin gelatin (Sigma-Aldrich) in PBS for 10 min, followed by incubation with the primary antibodies for Cxcr3 (1:100; R&D Systems) and/or Egfr (1:100, CST). Rhodamine red-conjugated anti-mouse (1:200) and FITC-conjugated anti-rabbit (1:100) secondary antibodies purchased from Jackson ImmunoResearch Laboratories (West Grove, PA) were used. Nuclei were stained with DAPI (Vector Labs) and cells were visualized using a confocal microscope, Zeiss LSM 880 (Zeiss, Oberkochen, Germany). Six to 10 field images were taken per condition at $\times$40 magnification. Confocal images were processed using the Zeiss Zen 3.1 microscope software and quantification of pixel intensities were determined using the Image J software (https://imagej.nih.gov/ij/). The JaCoP Plugin (https://imagej.nih.gov/ij/) was used to minimize the background labeling via the threshold selection function and calculate the Manders coefficients per image (46). In brief, the Manders coefficient M1 and M2 calculations were formulated by Manders et al. and are widely used to determine the fraction of one image channel's signal that overlaps with the signal from another channel, where:

$$\mathrm{M1} = \frac{\sum_i R_{i,\mathrm{coloc}}}{\sum_i R_i} \text{ and } \mathrm{M2} = \frac{\sum_i G_{i,\mathrm{coloc}}}{\sum_i G_i}$$

$R_{i,\mathrm{coloc}}$ and $G_{i,\mathrm{coloc}}$ represent the intensity of colocalized red and green pixels, respectively, while R_i and G_i are the total pixel intensities of each channel (47). This method of cooccurrence detection was designed to overcome the limitations of other colocalization detection methods such as the Pearson's correlation coefficient, which is a measure of covariance more appropriate for linear correlations and was shown more optimal for single cell measurements rather than field image analysis (48).

Breast tumor gene expression data set and statistical analysis. The GDS806 gene expression data set (49) was retrieved from Gene Expression Omnibus (www.ncbi.nih.gov). The METABRIC (50, 51) data set was downloaded from cBioPortal for Cancer Genomics (www.cbioportal.org) and The Cancer Genome Atlas (TCGA) data set was downloaded as described previously (15). The mean expression values of each gene were used as the cutoffs for comparing patient survival. Kaplan-Meier survival analyses were performed using the GraphPad Prism 8 software (GraphPad Software, San Diego, CA). For patient survival analyses, the log rank test was used; $P < 0.05$ was considered significant. Relationship between tumor distributions and molecular subtypes was analyzed using Fisher's Exact Probability test; $P < 0.05$ was considered significant. Dot plots and box and whisker plots were used to graph M1 coefficients for immunofluorescent colocalization. For cell assays and immunofluorescent quantifications, an unpaired 2-tailed Student's t test was used to determine statistical significance; $P < 0.01$ was considered significant.

ACKNOWLEDGMENTS

The study was funded by the Baylor Scott & White Research Institute (BSWRI) and Translational Genomics Research Institute (TGen) Oncology Research Collaboration Initiative grant CP-10 (to S.K.), University of Arizona College of Medicine—Phoenix Basic Medical Sciences COOP funding (to S.K.), the Fidelity Charitable Donor-Advised Yoo Family fund grant (to S.K.), and University of Arizona RDI Metastatic Breast Cancer funding (to J.A.S. and S.K.). Emily Peterson contributed to the study as an Arizona State University Barrett Honor's College student. Emily Tsutsusmi was supported by the TGen Helios Education Foundation for a summer. We thank Chelsea Claw, who was supported by the Youth Enjoy Science (YES)

grant (NIH/NCI R25CA221777, U Nebraska) and subsequently by the Partnership for Native American Cancer Prevention (NACP) program grant (NIH/NCI U54CA143924, U Arizona Cancer Center), for her technical support with Western blots.

E.T., J.S., and E.A.P. performed migration assays and Western blots. E.T. performed immunofluorescent staining and calculated Manders coefficients. E.T. and S.K. analyzed the results, performed statistics, and made figures. J.A.S. provided SAH-control and SAH-EJ1 peptides and her expert advice on the juxtamembrane domain of Egfr. E.T. and S.K. analyzed GDS806 and S.K. analyzed METABRIC and TCGA data sets. S.K. conceived the study, supervised the experiments, and wrote the manuscript. All authors contributed to the manuscript preparationand read and approved the final manuscript.

We have no conflicts of interest to declare.

REFERENCES

1. Metzemaekers M, Vanheule V, Janssens R, Struyf S, Proost P. 2017. Overview of the mechanisms that may contribute to the non-redundant activities of interferon-inducible CXC chemokine receptor 3 ligands. Front Immunol 8:1970. https://doi.org/10.3389/fimmu.2017.01970.
2. Weis WI, Kobilka BK. 2018. The molecular basis of G protein-coupled receptor activation. Annu Rev Biochem 87:897–919. https://doi.org/10.1146/annurev-biochem-060614-033910.
3. Tokunaga R, Zhang W, Naseem M, Puccini A, Berger MD, Soni S, McSkane M, Baba H, Lenz HJ. 2018. CXCL9, CXCL10, CXCL11/CXCR3 axis for immune activation: a target for novel cancer therapy. Cancer Treat Rev 63:40–47. https://doi.org/10.1016/j.ctrv.2017.11.007.
4. Do HTT, Lee CH, Cho J. 2020. Chemokines and their receptors: multifaceted roles in cancer progression and potential value as cancer prognostic markers. Cancers (Basel 12):287. https://doi.org/10.3390/cancers12020287.
5. Lee EY, Lee ZH, Song YW. 2013. The interaction between CXCL10 and cytokines in chronic inflammatory arthritis. Autoimmun Rev 12:554–557. https://doi.org/10.1016/j.autrev.2012.10.001.
6. Antonelli A, Ferrari SM, Giuggioli D, Ferrannini E, Ferri C, Fallahi P. 2014. Chemokine (C-X-C motif) ligand (CXCL)10 in autoimmune diseases. Autoimmun Rev 13:272–280. https://doi.org/10.1016/j.autrev.2013.10.010.
7. Trivedi PJ, Adams DH. 2018. Chemokines and chemokine receptors as therapeutic targets in inflammatory bowel disease: pitfalls and promise. J Crohns Colitis 12:1508. https://doi.org/10.1093/ecco-jcc/jjy130.
8. Shimada A, Oikawa Y, Yamada Y, Okubo Y, Narumi S. 2009. The role of the CXCL10/CXCR3 system in type 1 diabetes. Rev Diabet Stud 6:81–84. https://doi.org/10.1900/RDS.2009.6.81.
9. Roep BO, Kleijwegt FS, van Halteren AG, Bonato V, Boggi U, Vendrame F, Marchetti P, Dotta F. 2010. Islet inflammation and CXCL10 in recent-onset type 1 diabetes. Clin Exp Immunol 159:338–343. https://doi.org/10.1111/j.1365-2249.2009.04087.x.
10. Balkwill F. 2004. Cancer and the chemokine network. Nat Rev Cancer 4:540–550. https://doi.org/10.1038/nrc1388.
11. Jiang Z, Xu Y, Cai S. 2010. CXCL10 expression and prognostic significance in stage II and III colorectal cancer. Mol Biol Rep 37:3029–3036. https://doi.org/10.1007/s11033-009-9873-z.
12. Bronger H, Singer J, Windmuller C, Reuning U, Zech D, Delbridge C, Dorn J, Kiechle M, Schmalfeldt B, Schmitt M, Avril S. 2016. CXCL9 and CXCL10 predict survival and are regulated by cyclooxygenase inhibition in advanced serous ovarian cancer. Br J Cancer 115:553–563. https://doi.org/10.1038/bjc.2016.172.
13. Sato Y, Motoyama S, Nanjo H, Wakita A, Yoshino K, Sasaki T, Nagaki Y, Liu J, Imai K, Saito H, Minamiya Y. 2016. CXCL10 expression status is prognostic in patients with advanced thoracic esophageal squamous cell carcinoma. Ann Surg Oncol 23:936–942. https://doi.org/10.1245/s10434-015-4909-1.
14. Hilborn E, Sivik T, Fornander T, Stal O, Nordenskjold B, Jansson A. 2014. C-X-C ligand 10 and C-X-C receptor 3 status can predict tamoxifen treatment response in breast cancer patients. Breast Cancer Res Treat 145:73–82. https://doi.org/10.1007/s10549-014-2933-7.
15. Hendricks WPD, Briones N, Halperin RF, Facista S, Heaton PR, Mahadevan D, Kim S. 2019. PD-1-associated gene expression signature of neoadjuvant trastuzumab-treated tumors correlates with patient survival in HER2-positive breast cancer. Cancers (Basel) 11:1566. https://doi.org/10.3390/cancers11101566.
16. Adams S, Diamond JR, Hamilton E, Pohlmann PR, Tolaney SM, Chang CW, Zhang W, Iizuka K, Foster PG, Molinero L, Funke R, Powderly J. 2019. Atezolizumab plus nab-paclitaxel in the treatment of metastatic triple-negative breast cancer with 2-year survival follow-up: a phase 1b clinical trial. JAMA Oncol 5:334–342. https://doi.org/10.1001/jamaoncol.2018.5152.
17. Tumeh PC, Harview CL, Yearley JH, Shintaku IP, Taylor EJ, Robert L, Chmielowski B, Spasic M, Henry G, Ciobanu V, West AN, Carmona M, Kivork C, Seja E, Cherry G, Gutierrez AJ, Grogan TR, Mateus C, Tomasic G, Glaspy JA, Emerson RO, Robins H, Pierce RH, Elashoff DA, Robert C, Ribas A. 2014. PD-1 blockade induces responses by inhibiting adaptive immune resistance. Nature 515:568–571. https://doi.org/10.1038/nature13954.
18. Fernandez-Poma SM, Salas-Benito D, Lozano T, Casares N, Riezu-Boj JI, Mancheno U, Elizalde E, Alignani D, Zubeldia N, Otano I, Conde E, Sarobe P, Lasarte JJ, Hervas-Stubbs S. 2017. Expansion of tumor-infiltrating CD8(+) T cells expressing PD-1 improves the efficacy of adoptive T-cell therapy. Cancer Res 77:3672–3684. https://doi.org/10.1158/0008-5472.CAN-17-0236.
19. Karin N, Razon H. 2018. Chemokines beyond chemo-attraction: CXCL10 and its significant role in cancer and autoimmunity. Cytokine 109:24–28. https://doi.org/10.1016/j.cyto.2018.02.012.
20. Nagpal ML, Davis J, Lin T. 2006. Overexpression of CXCL10 in human prostate LNCaP cells activates its receptor (CXCR3) expression and inhibits cell proliferation. Biochim Biophys Acta 1762:811–818. https://doi.org/10.1016/j.bbadis.2006.06.017.
21. Antonicelli F, Lorin J, Kurdykowski S, Gangloff SC, Le Naour R, Sallenave JM, Hornebeck W, Grange F, Bernard P. 2011. CXCL10 reduces melanoma proliferation and invasiveness in vitro and in vivo. Br J Dermatol 164:720–728. https://doi.org/10.1111/j.1365-2133.2010.10176.x.
22. Mulligan AM, Raitman I, Feeley L, Pinnaduwage D, Nguyen LT, O'Malley FP, Ohashi PS, Andrulis IL. 2013. Tumoral lymphocytic infiltration and expression of the chemokine CXCL10 in breast cancers from the Ontario Familial Breast Cancer Registry. Clin Cancer Res 19:336–346. https://doi.org/10.1158/1078-0432.CCR-11-3314.
23. Lunardi S, Jamieson NB, Lim SY, Griffiths KL, Carvalho-Gaspar M, Al-Assar O, Yameen S, Carter RC, McKay CJ, Spoletini G, D'Ugo S, Silva MA, Sansom OJ, Janssen KP, Muschel RJ, Brunner TB. 2014. IP-10/CXCL10 induction in human pancreatic cancer stroma influences lymphocytes recruitment and correlates with poor survival. Oncotarget 5:11064–11080. https://doi.org/10.18632/oncotarget.2519.
24. Jiang H, Gebhardt C, Umansky L, Beckhove P, Schulze TJ, Utikal J, Umansky V. 2015. Elevated chronic inflammatory factors and myeloid-derived suppressor cells indicate poor prognosis in advanced melanoma patients. Int J Cancer 136:2352–2360. https://doi.org/10.1002/ijc.29297.
25. Wightman SC, Uppal A, Pitroda SP, Ganai S, Burnette B, Stack M, Oshima G, Khan S, Huang X, Posner MC, Weichselbaum RR, Khodarev NN. 2015. Oncogenic CXCL10 signalling drives metastasis development and poor clinical outcome. Br J Cancer 113:327–335. https://doi.org/10.1038/bjc.2015.193.
26. Maru SV, Holloway KA, Flynn G, Lancashire CL, Loughlin AJ, Male DK, Romero IA. 2008. Chemokine production and chemokine receptor expression by human glioma cells: role of CXCL10 in tumour cell proliferation. J Neuroimmunol 199:35–45. https://doi.org/10.1016/j.jneuroim.2008.04.029.
27. Ren T, Zhu L, Cheng M. 2017. CXCL10 accelerates EMT and metastasis by MMP-2 in hepatocellular carcinoma. Am J Transl Res 9:2824–2837.
28. Nozaki E, Kobayashi T, Ohnishi H, Ohtsuka K, Masaki T, Watanabe T, Sugiyama M. 2020. C-X-C motif receptor 3A enhances proliferation and invasiveness of colorectal cancer cells, and is mediated by C-X-C motif ligand 10. Oncol Lett 19:2495–2501. https://doi.org/10.3892/ol.2020.11326.

29. Wu X, Sun A, Yu W, Hong C, Liu Z. 2020. CXCL10 mediates breast cancer tamoxifen resistance and promotes estrogen-dependent and independent proliferation. Mol Cell Endocrinol 512:110866. https://doi.org/10.1016/j.mce.2020.110866.
30. Walser TC, Rifat S, Ma X, Kundu N, Ward C, Goloubeva O, Johnson MG, Medina JC, Collins TL, Fulton AM. 2006. Antagonism of CXCR3 inhibits lung metastasis in a murine model of metastatic breast cancer. Cancer Res 66:7701–7707. https://doi.org/10.1158/0008-5472.CAN-06-0709.
31. Ma X, Norsworthy K, Kundu N, Rodgers WH, Gimotty PA, Goloubeva O, Lipsky M, Li Y, Holt D, Fulton A. 2009. CXCR3 expression is associated with poor survival in breast cancer and promotes metastasis in a murine model. Mol Cancer Ther 8:490–498. https://doi.org/10.1158/1535-7163.MCT-08-0485.
32. Cambien B, Karimdjee BF, Richard-Fiardo P, Bziouech H, Barthel R, Millet MA, Martini V, Birnbaum D, Scoazec JY, Abello J, Al Saati T, Johnson MG, Sullivan TJ, Medina JC, Collins TL, Schmid-Alliana A, Schmid-Antomarchi H. 2009. Organ-specific inhibition of metastatic colon carcinoma by CXCR3 antagonism. Br J Cancer 100:1755–1764. https://doi.org/10.1038/sj.bjc.6605078.
33. Pradelli E, Karimdjee-Soilihi B, Michiels JF, Ricci JE, Millet MA, Vandenbos F, Sullivan TJ, Collins TL, Johnson MG, Medina JC, Kleinerman ES, Schmid-Alliana A, Schmid-Antomarchi H. 2009. Antagonism of chemokine receptor CXCR3 inhibits osteosarcoma metastasis to lungs. Int J Cancer 125:2586–2594. https://doi.org/10.1002/ijc.24665.
34. Lee JH, Kim HN, Kim KO, Jin WJ, Lee S, Kim HH, Ha H, Lee ZH. 2012. CXCL10 promotes osteolytic bone metastasis by enhancing cancer outgrowth and osteoclastogenesis. Cancer Res 72:3175–3186. https://doi.org/10.1158/0008-5472.CAN-12-0481.
35. Butler KL, Clancy-Thompson E, Mullins DW. 2017. CXCR3(+) monocytes/macrophages are required for establishment of pulmonary metastases. Sci Rep 7:45593. https://doi.org/10.1038/srep45593.
36. Byron SA, Min E, Thal TS, Hostetter G, Watanabe AT, Azorsa DO, Little TH, Tapia C, Kim S. 2012. Negative regulation of NF-kappaB by the ING4 tumor suppressor in breast cancer. PLoS One 7:e46823. https://doi.org/10.1371/journal.pone.0046823.
37. Shatnawi A, Ayoub NM, Alkhalifa AE. 2020. ING4 expression landscape and association with clinicopathologic characteristics in breast cancer. Clin Breast Cancer https://doi.org/10.1016/j.clbc.2020.11.011.
38. Doyon Y, Cayrou C, Ullah M, Landry AJ, Cote V, Selleck W, Lane WS, Tan S, Yang XJ, Cote J. 2006. ING tumor suppressor proteins are critical regulators of chromatin acetylation required for genome expression and perpetuation. Mol Cell 21:51–64. https://doi.org/10.1016/j.molcel.2005.12.007.
39. Hung T, Binda O, Champagne KS, Kuo AJ, Johnson K, Chang HY, Simon MD, Kutateladze TG, Gozani O. 2009. ING4 mediates crosstalk between histone H3 K4 trimethylation and H3 acetylation to attenuate cellular transformation. Mol Cell 33:248–256. https://doi.org/10.1016/j.molcel.2008.12.016.
40. Dantas A, Al Shueili B, Yang Y, Nabbi A, Fink D, Riabowol K. 2019. Biological Functions of the ING Proteins. Cancers (Basel) 11:1817. https://doi.org/10.3390/cancers11111817.
41. Garkavtsev I, Kozin SV, Chernova O, Xu L, Winkler F, Brown E, Barnett GH, Jain RK. 2004. The candidate tumour suppressor protein ING4 regulates brain tumour growth and angiogenesis. Nature 428:328–332. https://doi.org/10.1038/nature02329.
42. Nozell S, Laver T, Moseley D, Nowoslawski L, De Vos M, Atkinson GP, Harrison K, Nabors LB, Benveniste EN. 2008. The ING4 tumor suppressor attenuates NF-kappaB activity at the promoters of target genes. Mol Cell Biol 28:6632–6645. https://doi.org/10.1128/MCB.00697-08.
43. Sanjana NE, Shalem O, Zhang F. 2014. Improved vectors and genome-wide libraries for CRISPR screening. Nat Methods 11:783–784. https://doi.org/10.1038/nmeth.3047.
44. Shalem O, Sanjana NE, Hartenian E, Shi X, Scott DA, Mikkelson T, Heckl D, Ebert BL, Root DE, Doench JG, Zhang F. 2014. Genome-scale CRISPR-Cas9 knockout screening in human cells. Science 343:84–87. https://doi.org/10.1126/science.1247005.
45. Keenen MM, Kim S. 2016. Tumor suppressor ING4 inhibits estrogen receptor activity in breast cancer cells. Breast Cancer (Dove Med Press) 8:211–221. https://doi.org/10.2147/BCTT.S119691.
46. Bolte S, Cordelieres FP. 2006. A guided tour into subcellular colocalization analysis in light microscopy. J Microsc 224:213–232. https://doi.org/10.1111/j.1365-2818.2006.01706.x.
47. Manders EMM, Verbeek FJ, Aten JA. 1993. Measurement of co-localization of objects in dual-colour confocal images. J Microsc 169:375–382. https://doi.org/10.1111/j.1365-2818.1993.tb03313.x.
48. Dunn KW, Kamocka MM, McDonald JH. 2011. A practical guide to evaluating colocalization in biological microscopy. Am J Physiol Cell Physiol 300:C723–42. https://doi.org/10.1152/ajpcell.00462.2010.
49. Ma XJ, Wang Z, Ryan PD, Isakoff SJ, Barmettler A, Fuller A, Muir B, Mohapatra G, Salunga R, Tuggle JT, Tran Y, Tran D, Tassin A, Amon P, Wang W, Wang W, Enright E, Stecker K, Estepa-Sabal E, Smith B, Younger J, Balis U, Michaelson J, Bhan A, Habin K, Baer TM, Brugge J, Haber DA, Erlander MG, Sgroi DC. 2004. A two-gene expression ratio predicts clinical outcome in breast cancer patients treated with tamoxifen. Cancer Cell 5:607–616. https://doi.org/10.1016/j.ccr.2004.05.015.
50. Curtis C, Shah SP, Chin SF, Turashvili G, Rueda OM, Dunning MJ, Speed D, Lynch AG, Samarajiwa S, Yuan Y, Graf S, Ha G, Haffari G, Bashashati A, Russell R, McKinney S, Group M, Langerod A, Green A, Provenzano E, Wishart G, Pinder S, Watson P, Markowetz F, Murphy L, Ellis I, Purushotham A, Borresen-Dale AL, Brenton JD, Tavare S, Caldas C, Aparicio S, METABRIC Group. 2012. The genomic and transcriptomic architecture of 2,000 breast tumours reveals novel subgroups. Nature 486:346–352. https://doi.org/10.1038/nature10983.
51. Pereira B, Chin SF, Rueda OM, Vollan HK, Provenzano E, Bardwell HA, Pugh M, Jones L, Russell R, Sammut SJ, Tsui DW, Liu B, Dawson SJ, Abraham J, Northen H, Peden JF, Mukherjee A, Turashvili G, Green AR, McKinney S, Oloumi A, Shah S, Rosenfeld N, Murphy L, Bentley DR, Ellis IO, Purushotham A, Pinder SE, Borresen-Dale AL, Earl HM, Pharoah PD, Ross MT, Aparicio S, Caldas C. 2016. The somatic mutation profiles of 2,433 breast cancers refines their genomic and transcriptomic landscapes. Nat Commun 7:11479. https://doi.org/10.1038/ncomms11479.
52. Canver MC, Haeussler M, Bauer DE, Orkin SH, Sanjana NE, Shalem O, Yuan GC, Zhang F, Concordet JP, Pinello L. 2018. Integrated design, execution, and analysis of arrayed and pooled CRISPR genome-editing experiments. Nat Protoc 13:946–986. https://doi.org/10.1038/nprot.2018.005.
53. Johnson M, Li AR, Liu J, Fu Z, Zhu L, Miao S, Wang X, Xu Q, Huang A, Marcus A, Xu F, Ebsworth K, Sablan E, Danao J, Kumer J, Dairaghi D, Lawrence C, Sullivan T, Tonn G, Schall T, Collins T, Medina J. 2007. Discovery and optimization of a series of quinazolinone-derived antagonists of CXCR3. Bioorg Med Chem Lett 17:3339–3343. https://doi.org/10.1016/j.bmcl.2007.03.106.
54. Kim Y, Apetri M, Luo B, Settleman JE, Anderson KS. 2015. Differential effects of tyrosine kinase inhibitors on normal and oncogenic EGFR signaling and downstream effectors. Mol Cancer Res 13:765–774. https://doi.org/10.1158/1541-7786.MCR-14-0326.
55. Mezi S, Todi L, Orsi E, Angeloni A, Mancini P. 2012. Involvement of the Src-cortactin pathway in migration induced by IGF-1 and EGF in human breast cancer cells. Int J Oncol 41:2128–2138. https://doi.org/10.3892/ijo.2012.1642.
56. Harrison SM, Knifley T, Chen M, O'Connor KL. 2013. LPA, HGF, and EGF utilize distinct combinations of signaling pathways to promote migration and invasion of MDA-MB-231 breast carcinoma cells. BMC Cancer 13:501. https://doi.org/10.1186/1471-2407-13-501.
57. Appert-Collin A, Hubert P, Cremel G, Bennasroune A. 2015. Role of ErbB receptors in cancer cell migration and invasion. Front Pharmacol 6:283. https://doi.org/10.3389/fphar.2015.00283.
58. Kose M. 2017. GPCRs and EGFR: cross-talk of membrane receptors in cancer. Bioorg Med Chem Lett 27:3611–3620. https://doi.org/10.1016/j.bmcl.2017.07.002.
59. Salazar N, Munoz D, Kallifatidis G, Singh RK, Jorda M, Lokeshwar BL. 2014. The chemokine receptor CXCR7 interacts with EGFR to promote breast cancer cell proliferation. Mol Cancer 13:198. https://doi.org/10.1186/1476-4598-13-198.
60. Finlay-Schultz J, Jacobsen BM, Riley D, Paul KV, Turner S, Ferreira-Gonzalez A, Harrell JC, Kabos P, Sartorius CA. 2020. New generation breast cancer cell lines developed from patient-derived xenografts. Breast Cancer Res 22:68. https://doi.org/10.1186/s13058-020-01300-y.
61. Wosikowski K, Schuurhuis D, Kops GJ, Saceda M, Bates SE. 1997. Altered gene expression in drug-resistant human breast cancer cells. Clin Cancer Res 3:2405–2414.
62. Maisel SA, Broka D, Atwell B, Bunch T, Kupp R, Singh SK, Mehta S, Schroeder J. 2019. Stapled EGFR peptide reduces inflammatory breast cancer and inhibits additional HER-driven models of cancer. J Transl Med 17:201. https://doi.org/10.1186/s12967-019-1939-7.
63. Shahabuddin S, Ji R, Wang P, Brailoiu E, Dun N, Yang Y, Aksoy MO, Kelsen SG. 2006. CXCR3 chemokine receptor-induced chemotaxis in human airway epithelial cells: role of p38 MAPK and PI3K signaling pathways. Am J Physiol Cell Physiol 291:C34–9. https://doi.org/10.1152/ajpcell.00441.2005.
64. Billottet C, Quemener C, Bikfalvi A. 2013. CXCR3, a double-edged sword in tumor progression and angiogenesis. Biochim Biophys Acta 1836:287–295. https://doi.org/10.1016/j.bbcan.2013.08.002.
65. Fields TA, Casey PJ. 1997. Signalling functions and biochemical properties of pertussis toxin-resistant G-proteins. Biochem J 321:561–571. https://doi.org/10.1042/bj3210561.
66. Bonacci TM, Mathews JL, Yuan C, Lehmann DM, Malik S, Wu D, Font JL, Bidlack JM, Smrcka AV. 2006. Differential targeting of Gbetagamma-

subunit signaling with small molecules. Science 312:443–446. https://doi.org/10.1126/science.1120378.
67. Li J, Li G. 2010. Cell cycle regulator ING4 is a suppressor of melanoma angiogenesis that is regulated by the metastasis suppressor BRMS1. Cancer Res 70:10445–10453. https://doi.org/10.1158/0008-5472.CAN-10-3040.
68. Ibrahim EM, Al-Foheidi ME, Al-Mansour MM, Kazkaz GA. 2014. The prognostic value of tumor-infiltrating lymphocytes in triple-negative breast cancer: a meta-analysis. Breast Cancer Res Treat 148:467–476. https://doi.org/10.1007/s10549-014-3185-2.
69. Caldieri G, Malabarba MG, Di Fiore PP, Sigismund S. 2018. EGFR trafficking in physiology and cancer. Prog Mol Subcell Biol 57:235–272. https://doi.org/10.1007/978-3-319-96704-2_9.
70. Kirui JK, Xie Y, Wolff DW, Jiang H, Abel PW, Tu Y. 2010. Gbetagamma signaling promotes breast cancer cell migration and invasion. J Pharmacol Exp Ther 333:393–403. https://doi.org/10.1124/jpet.109.164814.
71. Tang X, Sun Z, Runne C, Madsen J, Domann F, Henry M, Lin F, Chen S. 2011. A critical role of Gbetagamma in tumorigenesis and metastasis of breast cancer. J Biol Chem 286:13244–13254. https://doi.org/10.1074/jbc.M110.206615.
72. Slamon DJ, Clark GM, Wong SG, Levin WJ, Ullrich A, McGuire WL. 1987. Human breast cancer: correlation of relapse and survival with amplification of the HER-2/neu oncogene. Science 235:177–182. https://doi.org/10.1126/science.3798106.
73. Brennan CW, Verhaak RG, McKenna A, Campos B, Noushmehr H, Salama SR, Zheng S, Chakravarty D, Sanborn JZ, Berman SH, Beroukhim R, Bernard B, Wu CJ, Genovese G, Shmulevich I, Barnholtz-Sloan J, Zou L, Vegesna R, Shukla SA, Ciriello G, Yung WK, Zhang W, Sougnez C, Mikkelsen T, Aldape K, Bigner DD, Van Meir EG, Prados M, Sloan A, Black KL, Eschbacher J, Finocchiaro G, Friedman W, Andrews DW, Guha A, Iacocca M, O'Neill BP, Foltz G, Myers J, Weisenberger DJ, Penny R, Kucherlapati R, Perou CM, Hayes DN, Gibbs R, Marra M, Mills GB, Lander E, Spellman P, Wilson R, TCGA Research Network, et al. 2013. The somatic genomic landscape of glioblastoma. Cell 155:462–477. https://doi.org/10.1016/j.cell.2013.09.034.
74. Hirsch FR, Varella-Garcia M, Bunn PA, Di Maria MV, Veve R, Bremnes RM, Barón AE, Zeng C, Franklin WA. 2003. Epidermal growth factor receptor in non-small-cell lung carcinomas: correlation between gene copy number and protein expression and impact on prognosis. JCO 21:3798–3807. https://doi.org/10.1200/JCO.2003.11.069.
75. Wang QS, Li M, Zhang LY, Jin Y, Tong DD, Yu Y, Bai J, Huang Q, Liu FL, Liu A, Lee KY, Fu SB. 2010. Down-regulation of ING4 is associated with initiation and progression of lung cancer. Histopathology 57:271–281. https://doi.org/10.1111/j.1365-2559.2010.03623.x.
76. Tapia C, Zlobec I, Schneider S, Kilic E, Guth U, Bubendorf L, Kim S. 2011. Deletion of the inhibitor of growth 4 (ING4) tumor suppressor gene is prevalent in human epidermal growth factor 2 (HER2)-positive breast cancer. Hum Pathol 42:983–990. https://doi.org/10.1016/j.humpath.2010.10.012.